GLUCOSE SENSING USING CADMIUM HYDROXIDE NANOWIRES

Dissertation submitted to
Visvesvaraya National Institute of Technology, Nagpur
In partial fulfillment of the requirements for the award of the degree

Master of Science

in

Physics

by

Astha Asati

(MS23PHY019)

Under the guidance of

Dr. Babasaheb R. Sankapal

Department of Physics
Visvesvaraya National Institute of Technology
Nagpur 440010 (India)

May 2025

GLUCOSE SENSING USING CADMIUM HYDROXIDE NANOWIRES

Dissertation submitted to
Visvesvaraya National Institute of Technology, Nagpur
In partial fulfillment of the requirements for the award of the degree

Master of Science

in

Physics

by

Astha Asati

(MS23PHY019)

Under the guidance of

Dr. Babasaheb R. Sankapal

Department of Physics
Visvesvaraya National Institute of Technology
Nagpur 440010 (India)

May 2025

© Visvesvaraya National Institute of Technology (VNIT) 2025

Department of Physics

Visvesvaraya National Institute of Technology,

Nagpur

Declaration

I, Astha Asati, hereby declare that this dissertation titled "**GLUCOSE SENSING USING CADMIUM HYDROXIDE NANOWIRES**" is carried out by me in the Department of Physics of Visvesvaraya National Institute of Technology, Nagpur. The work is original and has not been submitted earlier whole or in part for the award of any degree/diploma at this or any other Institution / University.

Astha Asati

Date:

Certificate

This to certify that the dissertation titled "**GLUCOSE SENSING USING CADMIUM HYDROXIDE NANOWIRES**" is submitted by **Astha Asati** in partial fulfillment of the requirements for the award of the degree of **Master of Science in Physics**, VNIT Nagpur. The work is comprehensive, complete and fit for final evaluation.

Dr. Babasaheb R. Sankapal

Professor

Department Of Physics

VNIT, Nagpur

Head, Department of Physics

VNIT, Nagpur

Date:

Department of Physics
Visvesvaraya National Institute of Technology, Nagpur

Non-Plagiarism Certificate

Certified that M.Sc. Dissertation titled "**GLUCOSE SENSING USING CADMIUM HYDROXIDE NANOWIRES**" submitted by **Astha Asati**, Enrollment No. **MS23PHY019**, ID No. **30652,** has been checked for plagiarism using TURNITIN software, and an overlap is found within prescribed limits (<30%). A summary of the report is given below:

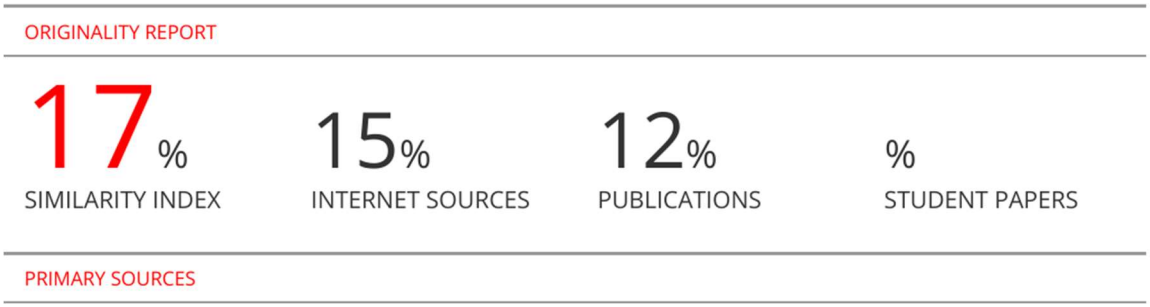

Astha Asati
(MS23PHY019)
ID No. 30652

Dr. Babasaheb R. Sankapal,
Associate Professor
Department of Physics
VNIT, Nagpur

ACKNOWLEDGEMENTS

I would like to begin by thanking the Almighty for his continuous guidance, generous blessings, and unending grace. Without his divine support, the successful completion of this project would not have been possible.

I would like to sincerely thank my project supervisor, ***Dr. B. R. Sankapal****, for accepting me as his M.Sc. project student and for his invaluable support, insightful guidance, and constant encouragement. His mentorship, patience during difficult phases, and generous support in terms of time, ideas, and resources played a pivotal role in the successful completion of this dissertation.*

My heartfelt thanks go to ***Ms. Swapna Rout****, a member of my project progress committee, for her thoughtful suggestions, critical evaluations, and valuable feedback, which significantly enhanced the quality of my experimental work and research progress.*

I am also grateful to ***Professor Prem Lal Patel****, Director, VNIT, Nagpur, for providing the necessary research infrastructure, including laboratory, library, and characterization facilities, which were instrumental in the execution of my project.*

I extend my thanks to all the ***faculty members of the Department of Physics*** *for their constant support and willingness to help whenever approached during different stages of the project. I am also thankful to* ***DST-FIST project (SR/FST/PSI/2017/5(C))*** *for the characterization.*

On a personal note, I would like to express my immense love and gratitude to my mother, Mrs. Anita Asati, whose unwavering belief in me, emotional strength, and endless sacrifices have been the backbone of my journey. She is truly my greatest inspiration. I am equally thankful to my father, Mr. Ram Kumar Asati, for his constant encouragement and moral support, and to my brother, Shashank Asati, for always being there to uplift my spirits during challenging times.

Thank you

Astha Asati

ABSTRACT

The progress of efficient, affordable, and scalable electrode materials for glucose sensing is crucial for advancing non enzymatic biosensor technologies. In this work, cadmium hydroxide $Cd(OH)_2$ thin films were easily synthesized using a simple chemical bath deposition (CBD) technique on a stainless-steel substrate (SS). This method offers low-temperature processing, affordability, and potential for industrial scalability. The synthesized $Cd(OH)_2$ films were characterized using X-ray diffraction (XRD) to confirm their crystalline structure and phase purity. FESEM with EDX were used to carried out the nanostructure morphology revealing a idea for electrochemical applications with individual element present in the sample. Fourier transform infrared spectroscopy (FTIR) was employed to identify the functional groups present, further confirming the formation of $Cd(OH)_2$. The electrochemical behavior of the $Cd(OH)_2$ electrode towards glucose detection was studied using cyclic voltammetry (CV) and amperometric analysis, demonstrating good sensitivity, fast response time, and reliable repeatability. The results suggest that $Cd(OH)_2$ synthesized via chemical bath deposition on stainless steel is a potential candidate for non enzymatic glucose sensing applications

LIST OF FIGURES

Figure no.	Figure title	Page no.
1.1	Various glucose sensing methods	2
1.2	Classification of glucose sensors into enzymatic and non enzymatic types.	4
1.3	Three generations of enzymatic glucose sensors	5
1.4	Redox-mediated electrocatalytic cycle in non enzymatic glucose sensing	7
1.5	Work plan	10
2.1	Classifications of thin film techniques	12
2.2	Experimental set up for chemical bath deposition method	13
2.3	Schematic of X-ray diffraction	15
2.4	Schematic of fourier transform infrared spectroscopy	16
2.5	Schematic of scanning electron microscope	17
2.6	Schematic of experimental set-up with three-electrode configuration	18
2.7	Cyclic voltammogram (CV)	20
2.8	Electrochemical impedance spectroscopy	21
2.9	Current time (i-t) amperometric curve	22
3.1	(a) Stainless steel substrate (SS) (b) SS/ $Cd(OH)_2$	25
3.2	XRD spectra of $Cd(OH)_2$	26
3.3	FTIR spectra of $Cd(OH)_2$	28

3.4	FESEM image of $Cd(OH)_2$ thin film	29
3.5	EDX spectra of $Cd(OH)_2$	29
3.6	(a) Electrolyte variation at the concentration of 1 M, (b) Concentration variation of the NaCl electrolyte, (c) CV curves at various scan rates in 1 M NaCl,(d) Peak current vs square root of scan rate in 1 M NaCl	31
3.7	a) CV response of SS/$Cd(OH)_2$ thin film at different concentration of glucose in 1M NaCl Solution & (b) a linear relationship between anodic peak current density and glucose concentration	32
3.8	Current time (i-t) amperometric curve of $Cd(OH)_2$ with successive addition of glucose in 1 M NaCl	32
3.9	Nyquist plot of bare electrode and addition of 1 mM glucose in 1 M NaCl	33
3.10	(a) CV response of SS/$Cd(OH)_2$ thin film towards glucose selectivity w.r.t fructose, sucrose (b) Variation of current density with concentration for different selective elements	34
3.11	Current time (i-t) amperometric curve of $Cd(OH)_2$ in presence of fructose, sucrose at a concentration of 1 mM in 1 M NaCl electrolyte	35

LIST OF TABLES

Table No.	Table title	Page no.
1	Literature survey of non enzymatic glucose sensor	8
3.1	X-ray diffraction peaks position and plane	27
3.2	Elemental composition of $Cd(OH)_2$	30
3.3	Impedance parameters	34
4.1	Maximum anodic current of $Cd(OH)_2$ in different electrolytes at 100 mV/s	38
4.2	Maximum anodic current of $Cd(OH)_2$ in different concentration of NaCl	38
4.3	Maximum anodic current of $Cd(OH)_2$ with different scan rates	39
4.4	Maximum anodic current of $Cd(OH)_2$ in different concentration of glucose	40
4.5	Maximum anodic current of $Cd(OH)_2$ in various selective elements	40
4.6	Impedance parameters	41

INDEX

Sr. No	Title	Page No.
	CHAPTER I **GENERAL INTRODUCTION AND LITERATURE SURVEY**	
1.1	General introduction	1
1.2	Glucose sensing methods 1.2.1 Blood glucose meters (Invasive) 1.2.2 Continuous glucose monitors (CGM) 1.2.3 Non invasive glucose sensors 1.2.4 Wearable and implantable sensors 1.2.5 Electrochemical glucose biosensors	 2 2 3 3 3
1.3	Categorization based on sensing mechanism 1.3.1 Enzymatic glucose sensor 1.3.2 Non enzymatic glucose sensor	4 4 5
1.4	Material selection	7
1.5	Properties of cadmium hydroxide	8
1.6	Objectives	9
1.7	Work plan	10

CHAPTER II

BASIC CONCEPTS OF CHEMICAL BATH DEPOSITION METHODS, CHARACTERIZATION TECHNIQUES, AND GLUCOSE SENSING

2.1	Introduction	11
2.2	Classification of thin films	12
2.3	Chemical bath deposition method 2.3.1 Deposition process 2.3.2 Advantages of chemical bath deposition (CBD) 2.3.3 Disadvantages of chemical bath deposition (CBD)	12 13 14 14
2.4	Thin film characterizations techniques 2.4.1 X-ray diffraction techniques 2.4.2 Fourier transform infrared spectroscopy 2.4.3 Scanning electron microscope	14 15 16 17
2.5	Electrochemical studies 2.5.1 Electrochemical experimental setup to test the performance of glucose sensor 2.5.2 Cyclic voltammetry	18 18 19

	2.5.3 Electrochemical impedance spectroscopy	21
	2.5.4 Current time (i-t) amperometry	22

CHAPTER III

CADMIUM HYDROXIDE THIN FILM BY CHEMICAL BATH DEPOSITION METHOD FOR GLUCOSE SENSING APPLICATION

3.1	Introduction	23
3.2	Experimental details	23
	3.2.1 Materials	24
	3.2.2 Synthesis of cadmium hydroxide based thin film	24
	a) Substrate selection and cleaning process	24
	b) Material preparation	25
	3.2.3 Thin film on stainless steel by chemical bath deposition method.	
3.3	Characterizations	26
3.4	Results and discussions	26
	3.4.1 X-ray diffraction analysis (XRD)	26
	3.4.2 Fourier transform infrared spectroscopy (FTIR)	27
	3.4.3 Surface morphological studies	28
	3.4.3.1 Energy dispersive X-ray spectroscopy	29

3.5	Electrochemical analysis	30
	3.5.1 Sensitivity study	30
	3.5.1.1 Cyclic voltammetry	30
	3.5.1.2 Current time (i-t) amperometry	32
	3.5.1.3 Electrochemical impedance spectroscopy	33
	3.5.2 Selectivity study	34
	3.5.2.1 Cyclic voltammetry	34
	3.5.2.2 Current time (i-t) amperometry	35
	CHAPTER IV	
	SUMMARY AND CONCLUSIONS	
4.1	Introduction	36
4.2	Results and discussion	37
	4.2.1 Characterization analysis	37
	4.2.1.1 X-ray diffraction (XRD)	37
	4.2.1.2 Fourier transform infrared spectroscopy (FTIR)	37
	4.2.1.3 Scanning electron microscopy (SEM)	37
	4.2.1.4 Electrochemical study	38
4.3	Conclusions	41

CHAPTER I
GENERAL INTRODUCTION AND LITERATURE SURVEY

1.1 General introduction

Glucose sensing is important in the treatment of a variety of medical disorders, most notably diabetes, a chronic metabolic ailment indicated by the incapacity of the body to control blood glucose levels.

These tools are essential for tracking blood sugar levels, enhancing patient care, and guaranteeing improved health results. These sensors allow for prompt actions by continually monitoring glucose levels, thereby averting major consequences associated with abnormal blood sugar levels [1].

Glucose sensing methods range from basic blood glucose meters to sophisticated continuous glucose monitoring (CGM) systems. Each type is intended to meet a specific demand, such as daily monitoring or long-term glucose fluctuation tracking. In the larger framework of healthcare, glucose sensing is crucial for delivering vital information that informs tailored treatments and improved illness management. It is not simply about convenience. Millions of individuals throughout the world rely on these devices to improve their quality of life and lower their risk of complications from diabetes [2].

As there is a greater demand for more precise, non-invasive, and real-time glucose monitoring, the technology behind glucose sensors advances. The efficiency, accessibility, and usability of glucose sensing devices are increasing due to developments in engineering, materials science, and sensor design. However, accuracy, comfort, cost, and longevity remain key problems that researchers and developers are attempting to tackle. Amidst these challenges, the capacity for glucose sensing to transform healthcare is substantial. Researchers are committed to enhancing glucose monitoring systems by fostering continuous innovation and collaboration, with the objectives of increasing reliability, reducing costs, and ensuring broader accessibility. The ultimate aim is to advance diabetes

management, improve patient outcomes, and promote a healthier future for those affected by diabetes and other glucose-related health issues [3].

1.2 Glucose sensing methods

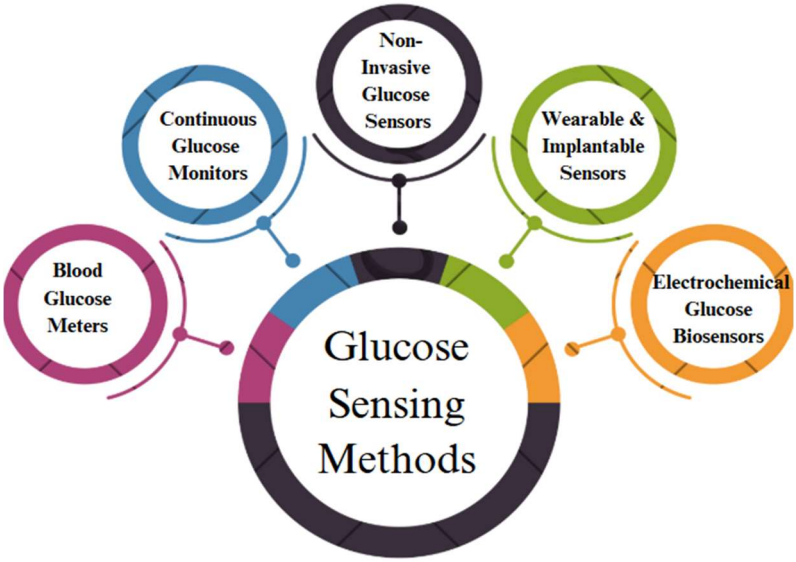

Fig 1.1 Various glucose sensing methods

1.2.1 Blood glucose meters (Invasive)

- **Description:** The most common glucose sensors used for routine monitoring.
- **How they work:** Requires a blood sample acquired through a fingertip prick. A sample of blood is applied to the test strip with enzymes that react with glucose, producing an electrical signal, which is then measured by the meter.

1.2.2 Continuous glucose monitors (CGM)

- **Description**: Devices that provide constant, instantaneous tracking of blood glucose throughout the day and night.
- **How they work**: A small sensor is placed under the skin (usually on the abdomen or arm) to measure glucose in interstitial fluid. Data is sent to a receiver, providing continuous readings and trends.

1.2.3 Non-invasive glucose sensors

- **Description**: These sensors aim to measure glucose levels without the need for blood or interstitial fluid samples.
- **How they work**: Various methods, such as optical, electromagnetic, or thermal techniques, are used to detect glucose through the skin or other body tissues.

1.2.4 Wearable and implantable sensors

- **Description:** Wearable sensors, like patches or smartwatches, offer non-invasive continuous glucose monitoring. Implantable sensors, placed under the skin, provide long-term glucose tracking with minimal maintenance.
- **How they work:** Wearable sensors monitor glucose in interstitial fluid and transmit data to a device. Implantable sensors also measure glucose in interstitial fluid, sending data wirelessly. Implantable sensors typically last longer, offering months of continuous monitoring.

1.2.5 Electrochemical glucose biosensors

- **Description:** These sensors use an electrochemical reaction to detect glucose levels and are commonly used in both blood glucose meters and CGMs.
- **How they work:** The enzyme or chemical reacts with glucose in the blood, producing an electrical current. The strength of the current is varying with the glucose concentration, which is measured to determine the glucose level [4].

1.3 Categorization based on sensing mechanism (Enzymatic vs. non enzymatic)

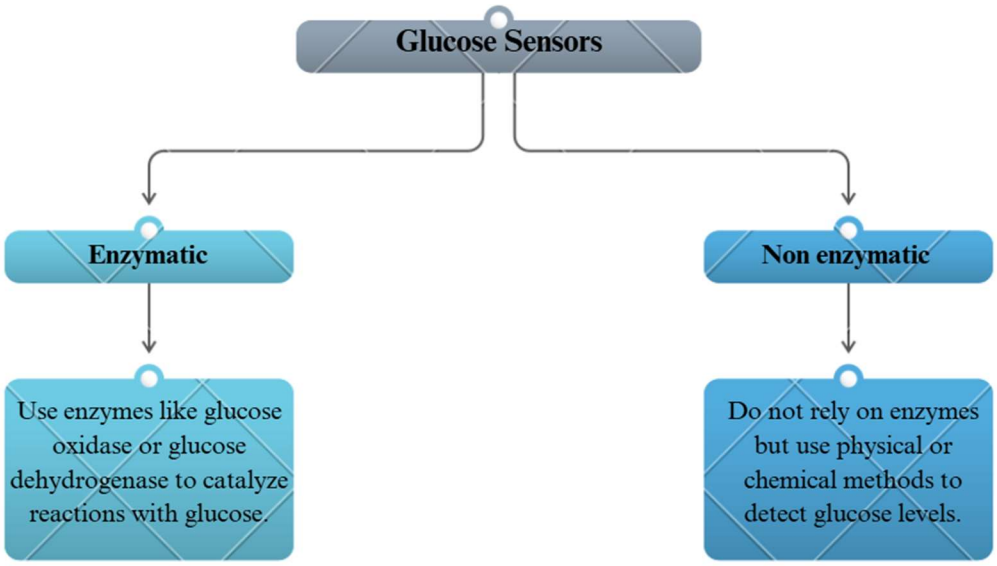
Glucose Sensors
Enzymatic
Non enzymatic
Use enzymes like glucose oxidase or glucose dehydrogenase to catalyze reactions with glucose.
Do not rely on enzymes but use physical or chemical methods to detect glucose levels.

Fig 1.2 Classification of glucose sensors into enzymatic and non enzymatic types.

After covering the general types, explaining the underlying technology:

1.3.1 Enzymatic glucose sensor

For a very long period, enzymes are the primary elements for designing of glucose sensors because of their known glucose processing mechanisms which serve as a chemical basis. The rapid reaction of biological enzymes with glucose is facilitated by their rate at which they catalyze reactions, facilitating an energetically favorable pathway for glucose oxidation. Among the various enzyme families linked to glucose metabolism, glucose oxidase & glucose dehydrogenases is widely recognized [5].

Enzyme-catalyzed reaction is given as follows:

$$\text{Glucose} + O_2 + GO_x \rightarrow \text{Gluconic acid} + H_2O_2 \qquad (1.1)$$

Depending on the type of oxidation mediator, we have three generations of glucose enzymatic sensor

Oxygen is used as a physiological mediator - first

Artificial (synthetic) electron acceptor- the second-generation

An electrode enabling direct electrical interfacing without mediators - the third-generation

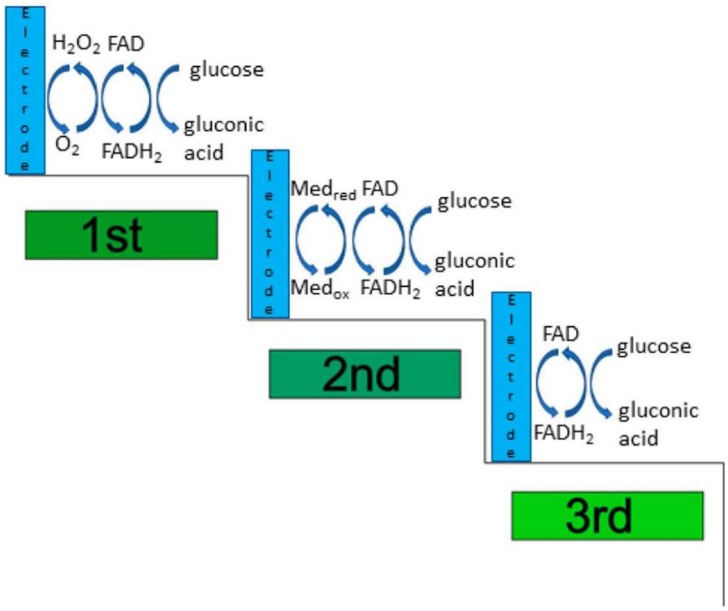

Figure 1.3 Three generations of enzymatic glucose sensors [6]

The enzymatic glucose sensor has good sensitivity & excellent selectivity but do have following disadvantages,

- Enzyme immobilization process, leads to disturb its reproducibility nature.
- Poor long-term stability
- The efficacy of these is being largely affected by external parameters including humidity, pH, and shifts in temperature causing elevated storage costs.
- Low repeatability
- Needs complicated manufacturing techniques
- Tough performance
- Glucose oxidase has poor chemical and thermal stability.

The disadvantages consequently constrain the application of enzyme-based sensors [7], [8], [9] [10].

1.3.2 Non enzymatic glucose sensor

Non enzymatic glucose sensors improve operational stability, shelf-life, and resistance to temperature or pH fluctuations by directly electro oxidizing glucose at a catalytically active electrode surface, doing away with the need for biological enzymes like glucose oxidase. Under an applied potential, glucose molecules undergo an oxidation reaction after adhering to a nanostructured electrocatalyst, which is often a metal (Ni, Cu, Pt), metal oxide (NiO, CoO_4) or bimetallic

composite. Quantitative analysis is made possible by the resultant current, which is varying with the glucose concentration. They are ideal for on-site testing and real-time monitoring systems due to their quick reaction times, broad linear detection ranges (from micromolar to millimolar values), and low detection limits. Non enzymatic sensors use high-surface-area nanostructures, like core-shell nanoparticles, nanowires, or nanoporous films, to improve mass transport and active site density and attain high sensitivity and selectivity [11].

The sensing process proceeds via a cyclical three-step redox shuttle between two oxidation states of the metal center as follows:

1. **Electrochemical activation of the catalyst**

   Under an applied potential between working electrode (WE) vs. reference electrode (Ag/AgCl), the metal active sites on the electrode surface are oxidized from a lower valence state (X^{2+}) to a higher valence state (X^{3+}):

$$X^{2+} \xrightarrow{e^- \text{at electrode}} X^{3+} \qquad (1.2)$$

2. **Chemical oxidation of glucose**

   The generated X^{3+} species act as chemical oxidants toward glucose molecules in solution. Glucose ($C_6H_{12}O_6$) is converted into gluconolactone ($C_6H_{10}O_6$), while X^{3+} is reduced back to X^{2+}:

$$C_6H_{12}O_6 + X^{3+} \xrightarrow{\text{yields}} C_6H_{10}O_6 + X^{2+} + 2\,H^+ \qquad (1.3)$$

3. **Electrochemical regeneration of the catalyst**

   The reduced X^{2+} species diffuse back to the electrode interface, where they are re-oxidized to X^{3+}, completing the catalytic cycle and sustaining a continuous anodic current:

$$X^{2+} \xrightarrow{e^- \text{at electrode}} X^{3+} \qquad (1.4)$$

As each glucose oxidation event consumes X^{3+} and forces its regeneration at the electrode, the magnitude of the anodic current rises in direct proportion to the glucose concentration.

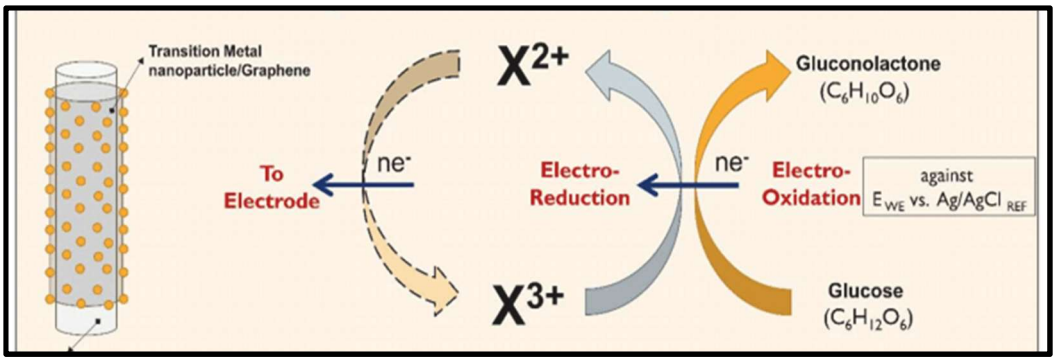

Figure 1.4 Redox-mediated electrocatalytic cycle in non enzymatic glucose sensing [12].

1.4 Material selection

High sensitivity enzyme-free glucose sensors need to utilize active ingredients with strong electrocatalytic activity. The pressing demand for glucose-monitoring systems has driven significant efforts toward the conception of next-generation sensors that combine high accuracy and sensitivity with affordability, rapid response times, outstanding selectivity, and dependable performance. The surface area, microstructure, and composition of nanomaterials greatly influence the non enzyme glucose sensors' sensing capabilities [13].

Utilizing the exceptional physical and chemical analytical qualities of nanostructural materials which have huge specific surface areas and increased catalytic activities, they are progressively used in creation of non enzymatic sensors. Enhancing glucose sensors anti-interference capability is important since selectivity plays a significant role in their analytical properties [14].

Research and development efforts are presently focused on creating more advanced materials with innovative morphologies that elevate every sensor criterion without sacrificing any, as the electrode surface is crucial in the design of non enzymatic glucose sensors [15].

In order to overcome these difficulties, scientists have resorted to using nanoporous materials, which are perfect for electrochemical sensing applications due to their

special qualities like increased surface area, adjustable pore size, and improved mass transport [16].

S.No.	Electrode Material	Substrate	Synthesis process	Electrolyte	Potential Window (V)	Morphology	Ref
1	Mn–La_2O_3	Stainless steel	Electrodeposition	0.1 M NaOH	0 to + 0.5	Nanoflakes	[17]
2	MoS_2/ NiNPs	Stainless steel	Electrodeposition	0.1 M NaOH	-0.2 to +0.8	Nanotubes	[18]
3	Co-Ni hydroxide	Graphite sheets	Electrodeposition	0.5M NaOH	0.0 to 0.55	Nanoflakes	[19]
4	CuO/ZnO	Glassy carbon	Hydrothermal method	0.5 M NaOH	0 to + 0.80	Nanoporous microsphere	[20]
5	NiO	Glassy carbon	Electrodeposition	0.1 M NaOH	0.2V to 1	Nanovesicle	[21]
6	Au film	ITO	Electrodeposition	0.1 M NaOH	-0.6 to 0.8	Three-dimensional porous structure	[22]

Table 1: Literature survey of non-enzymatic glucose sensor

1.5 Properties of cadmium hydroxide

- $Cd(OH)_2$ has a molar mass of 146.43 g/mol and exhibits a band gap of 3.2 eV. It is classified as an n-type material, which allows for quick electron transfer.
- It has monoclinic crystal structure.
- It's melting point and boiling point are 232 °C & 100 °C respectively.
- It's density is 4.79 g/cm^3.

1.5.1 Properties of cadmium

- The atomic number of cadmium is 48, present in group 12 and the d block of the periodic table has an electronic configuration [Kr] $4d^{10}$ $5s^2$.
- Cadmium exhibits +2 oxidation state and has an atomic mass of 112.411u.

1.6 Objective

- Coating of cadmium hydroxide $Cd(OH)_2$ by the chemical bath deposition method (CBD) on stainless steel (SS).
- Characterizations of $Cd(OH)_2$ by X-ray diffraction, scanning electron microscopy (SEM), fourier transform infrared spectroscopy (FTIR).
- Electrochemical study by cyclic voltammetry (CV) and electrochemical impedance spectroscopy (EIS).
- Current time (i-t) amperometry for detection of glucose and selectivity of glucose.

1.7 Work plan

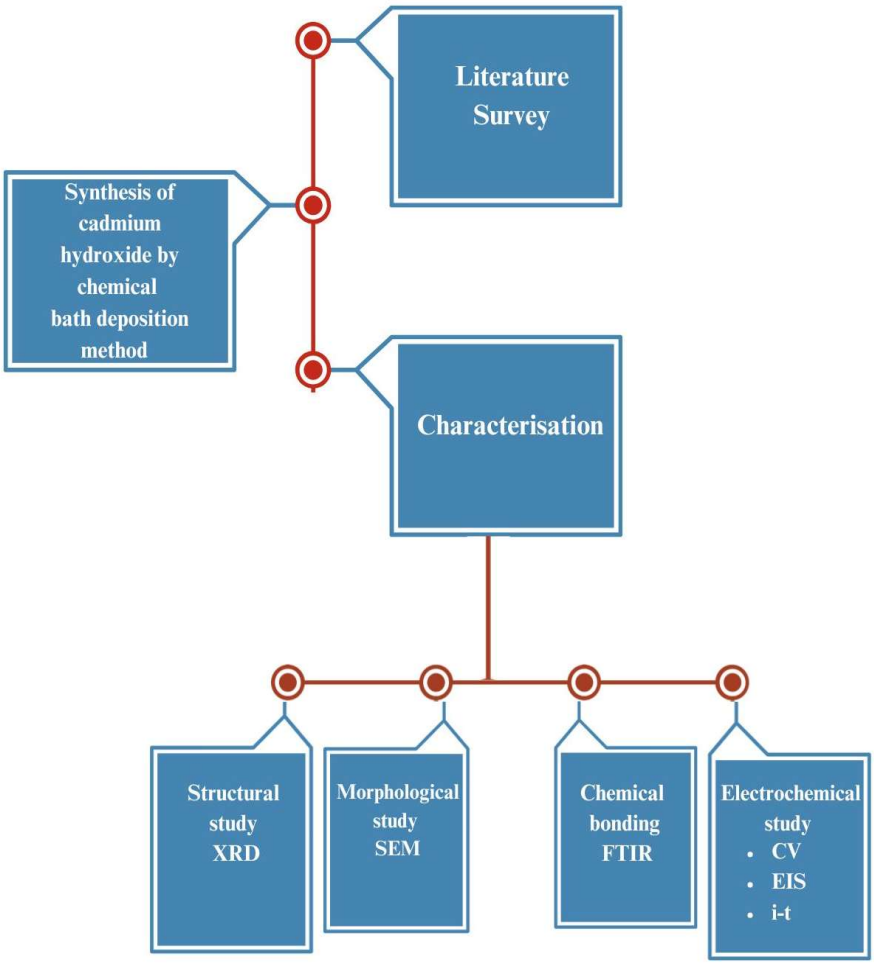

Fig.1.5 Work plan

CHAPTER II

BASIC CONCEPTS OF CHEMICAL BATH DEPOSITION METHODS, CHARACTERIZATION TECHNIQUES, AND GLUCOSE SENSING

2.1 Introduction

Several deposition methods have been utilized to develop nanostructured materials for glucose sensing, which is crucial for applications in biomedical diagnostics and monitoring. The choice of deposition technique is influenced not only by the desired sensing properties but also by the scalability and cost-effectiveness of the process. These synthesis methods are typically divided into physical and chemical approaches. Physical methods approaches like sputtering are utilized to produce thin films or nanostructured layers which can improve the electrochemical properties needed for glucose detection. However, these methods face challenges such as high equipment costs, low production rates, and difficulty in controlling the material's size, shape, and chemical composition, which can affect the accuracy and sensitivity of glucose sensors. In contrast, chemical deposition methods enable the controlled deposition of nanomaterials with precise morphology, structure, and functionalization, which are essential for improving the sensitivity and selectivity of glucose sensors. Furthermore, chemical deposition processes typically operate at lower temperatures and are more adaptable for scaling up, making them highly attractive for commercial production. Methods like electrodeposition and chemical bath deposition (CBD) are particularly promising because they allow for fine-tuning of the material properties to achieve optimal sensor performance while maintaining cost efficiency and scalability [19].

2.2 Classification of thin films

There are various methods available for thin film deposition, depending on the specific requirements. These techniques are mainly classified into two categories: physical deposition and chemical deposition. Physical methods involve the vaporization of source material molecules to form thin films, while chemical deposition involves chemical reactions with precursors that contain the film's components. The thin film deposition techniques can be further classified in several ways, as outlined below.

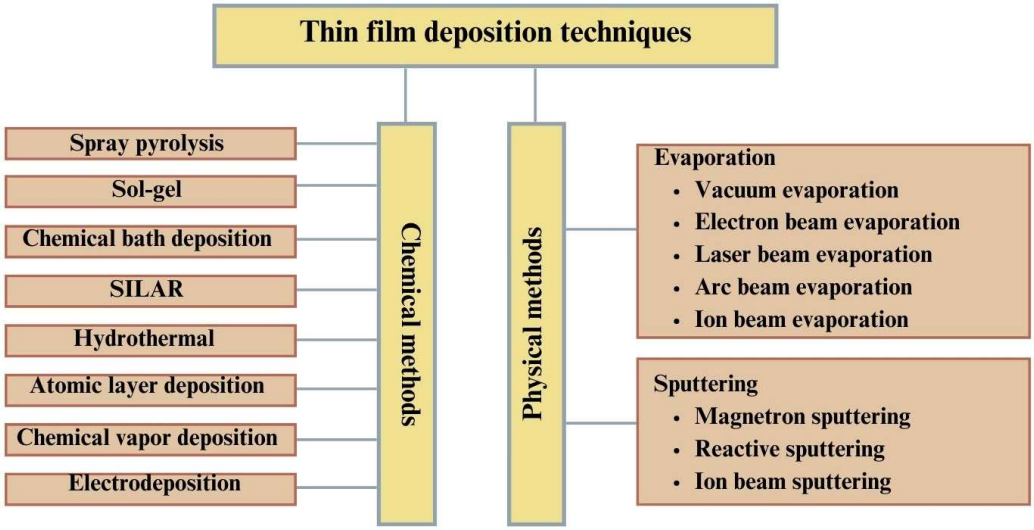

2.1 Classifications of thin film techniques

2.3 Chemical bath deposition method

The chemical bath deposition method involves the modulated formation of a desired compound from a solution onto an appropriate substrate. In this method, the film thickness and chemical composition can be regulated by adjusting deposition parameters like temperature, precursor concentration, the type of complexing agents, and the pH level of the solution [20].

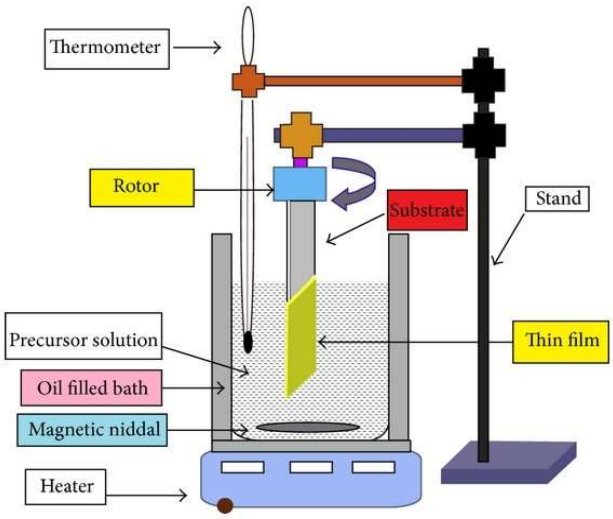

Fig 2.2 Experimental set up for chemical bath deposition method [20]

2.3.1 Deposition process

Substrate preparation:

The substrate is cleaned and treated to remove contaminants such as dust, oils, and oxides. Proper cleaning is essential to ensure good adhesion and uniformity of the thin film.

Precursor preparation:

Chemical precursors are mixed to form a homogeneous solution. This step may involve stirring or sonication to ensure uniform distribution of components for consistent film quality.

Substrate immersion:

The cleaned substrate is immersed into the prepared chemical bath where a thin layer forms on the substrate surface. The dipping speed, duration & temperature are controlled in order to obtain the required film thickness.

Drying of substrate

After deposition the substrate is withdrawn and dried under controlled conditions. This step helps evaporate any solvents and ensures the film adheres properly without forming cracks or defects [20].

2.3.2 Advantages of chemical bath deposition (CBD)

- **Cost-effective method:** CBD is affordable technique, making it accessible for both research and industrial applications.
- **Simple process:** The setup and procedure are straightforward, not requiring complex or high-vacuum equipment.
- **Low-temperature operation:** The process works effectively at relatively low temperatures, suitable for a wide range of substrates.
- **Atmospheric pressure conditions:** It does not require high-pressure environments, simplifying the overall system.
- **Scalable for large areas:** CBD can be easily adapted to coat large or multiple substrates, making it practical for mass production.

2.3.3 Disadvantages of chemical bath deposition (CBD)

- **Limited control over chemistry:** The lack of precise understanding of the reaction mechanisms restricts process flexibility and predictability.
- **Inefficient use of precursors:** A large portion of chemical reactants may go unused, making the process less efficient.
- **High waste generation:** The method produces considerable solvent and chemical waste, posing environmental and disposal concerns.
- **Unclear growth-material relationship:** There is insufficient explanation of how specific process parameters influence the final material structure and properties [21].

2.4 Thin film characterizations techniques

Nanoscale materials often possess properties that differ significantly from those of bulk materials. To ensure high performance and reliability, various analytical techniques are used to examine the properties of thin films. Characterization plays important role in validating the quality and functionality of the fabricated materials. It serves as a key bridge between scientific research and the development of innovative products. Through characterization, we gain insights into several critical aspects such as surface morphology, chemical composition, microstructural

features, and phase identification. In this section, we will provide a brief overview of the main techniques employed for thin film characterization.

2.4.1 X-ray diffraction techniques

X-ray diffraction is widely utilized method in determining a sample's crystalline structure or composition. It can be used to establish the atomic structure of larger crystals, such as inorganic materials and macromolecules. It can assess sample composition, crystallinity, and phase purity if the crystal size is excessively little. This method transmits X-rays through it. Since their wavelength corresponds to the distance between atoms in the material, X-ray beams are selected. This implies that the angle of diffraction will be influenced by the molecular atom spacing, as opposed to using much larger wavelengths, which would have no effect on the atom spacing. The X-rays subsequently traverse the specimen, scattering off the constituent atoms and causing the beam to deviate by an angle θ relative to its initial trajectory. This is the diffraction angle. However, when the diffracted waves share comparable wavelengths, they reinforce one another through constructive interference.

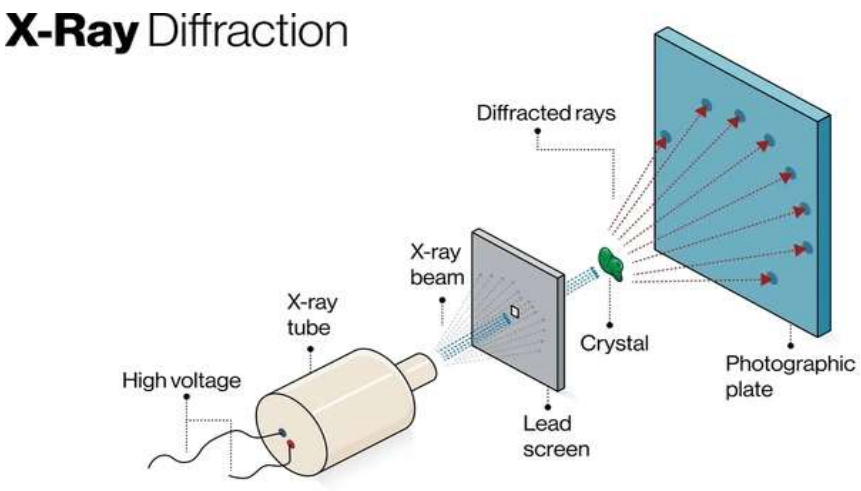

Fig 2.3 Schematic of X-ray diffraction [23]

Constructive interference arises when X-ray beams with phase differences corresponding to integer multiples of their wavelength merge, amplifying the resulting beam. For this particular diffraction angle, a larger wave amplitude means a stronger signal.

Bragg's law, $\sin\Theta=n\lambda/2d$, can then be utilized to calculate the difference between atomic planes from the diffraction angle, where d is the distance between atomic planes, θ is the angle of diffraction, and λ is the wavelength added. Composition or crystalline structure can then be deduced using the distance between atomic plates [23].

2.4.2 Fourier transform infrared spectroscopy (FTIR)

Fourier transform infrared spectroscopy (FTIR) is a spectroscopic process that analyzes wavelengths absorbed by substances using the mathematical technique of fourier transforms. In this method, a beam of light composed of multiple frequencies strikes the sample, and a data point is created by measuring how much of the beam the substance absorbs. This process of illuminating the light beam with different frequency combinations is accomplished by recording that specific point each time. The computer then analyzes these data points in reverse to assess absorption at each wavelength.

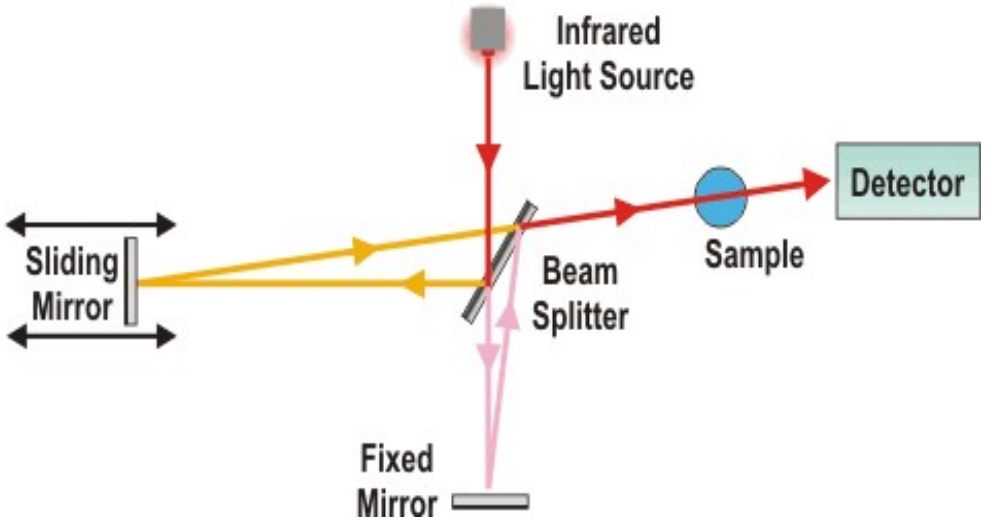

Fig 2.4 Schematic of fourier transform infrared spectroscopy [25]

The principle behind FTIR spectroscopy is that an interferogram is produced by means of radiation interference involving two beams. The latter is a signal generated as a result of the change in path length between the two beams that are reflected off two mirrors (located within the interferometer block). Fourier transform infrared spectroscopy gets its name owing to the fact that the two

domains of distance and frequency may be switched using the mathematical technique of fourier transformation [24].

2.4.3 Scanning electron microscope (SEM)

The Scanning electron microscope (SEM) is a kind of electron microscope that uses a low-energy electron beam to concentrate on and scan the surfaces of microorganisms. Electron microscopes were developed because light microscopes

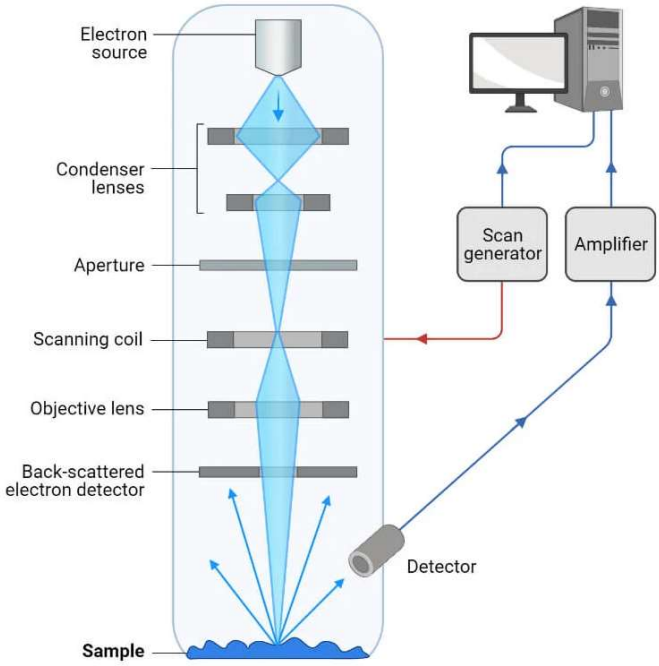

Fig. 2.5 Schematic of scanning electron microscope [26]

were inefficient due to their longer wavelengths. In contrast to light microscopes, electron microscopes have much shorter wavelengths, which allows for greater resolution.

The scanning electron microscope utilizes emitted electrons, in contrast to the transmission electron microscope, which involves transmitted electrons. The scanning electron microscope operates by applying kinetic energy to generate signals from electron interactions. These electrons, which are utilized to observe crystallized elements and photons, include secondary electrons, backscattered

electrons, and diffracted backscattered electrons. An image is created using secondary and backscattered electrons. While the backscattered electrons provide contrast in the specimen's elemental composition, the secondary electrons emitted by the specimen are primarily responsible for detecting its morphology and topography [26].

2.5 Electrochemical studies

Glucose sensing is a crucial application in biosensing technology: characterization, detection, and performance analysis play a vital role in optimizing glucose sensors. The primary electrochemical techniques employed for glucose sensing include cyclic voltammetry (CV), current time (i-t) amperometry, and electrochemical impedance spectroscopy (EIS). Through these electrochemical measurements, we can evaluate parameters such as sensitivity, limit of detection, and response time, which are essential for the advancement of accurate and reliable glucose sensing devices.

2.5.1 Electrochemical experimental setup to test the performance of glucose sensor

An electrochemical setup is commonly employed to evaluate the performance of glucose sensors. To investigate the sensing behavior of the electrode material, a three-electrode configuration is utilized in either aqueous or non-aqueous media. In contrast, a two-electrode system is adopted to assess the overall performance of the glucose sensing device [27].

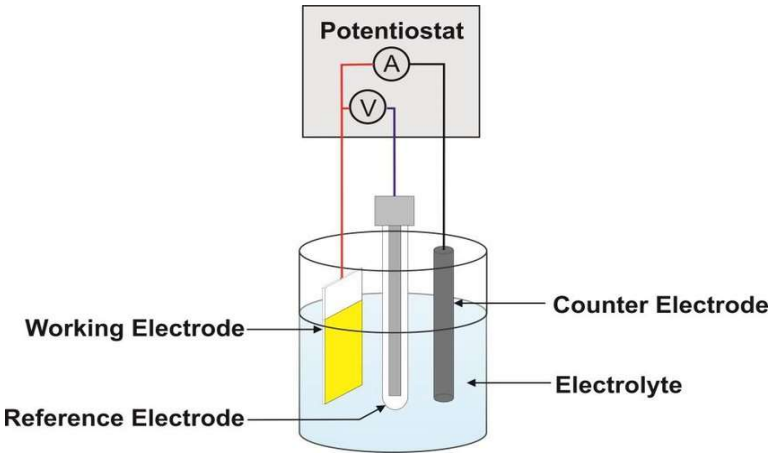

Fig 2.6 Schematic of experimental set-up with three-electrode configuration [28]

The electrochemical sensing performance was evaluated using working electrodes with fixed dimensions of 1 cm × 1 cm. Cyclic voltammetry (CV), current time (i-t) amperometry, and electrochemical impedance spectroscopy (EIS) measurements were conducted using gamry analyst software to analyze the glucose sensing characteristics.

2.5.2 Cyclic voltammetry

Cyclic voltammetry, an electrochemical technique, uses a potentiostat to record the current produced in response to redox activity within the solution as the applied potential is swept linearly over time. It is a helpful technique to know details about the kinetics of electronic-transfer reactions, analyte energy levels, and the thermodynamics of redox processes fast. This is crucial for characterizing fuel cell components, supercapacitors, battery materials, and conductive polymers. A working electrode, a reference electrode, and a counter electrode make up the three-electrode system used in cyclic voltammetry.

Electrolyte solution, a reference solution, and the three electrodes are added to an electrochemical cell in order to perform cyclic voltammetry. The voltage that exists between the reference and working electrodes should then be linearly swept using a potentiostat. The potentiostat will sweep back in the opposite way once it reaches the predetermined limit.

Throughout a scan, the potentiostat will carry out this procedure several times. The variation in current between the working and counter electrodes will be recorded throughout this process. The outcome is a **cyclic voltammogram**, which is a distinctive duck-shaped plot [29].

Cyclic voltammograms

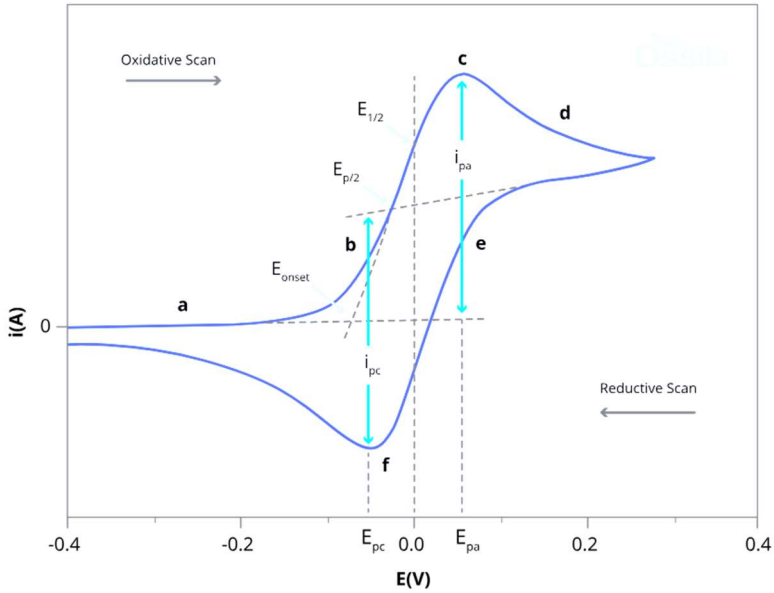

Fig. 2.7 Cyclic voltammogram (CV) [29]

The cyclic voltammogram refers to the 'duck-shaped' graph generated during cyclic voltammetry.

Depicted fig 2.7 is a cyclic voltammogram characteristic of an electrochemically reversible one-electron redox couple, in which the potential is initially held at – 0.4 V and then scanned anodically toward progressively more positive (oxidative) values. At first, the voltage is insufficient to cause the analyte to oxidize (a).

The onset (E_{onset}) of oxidation occurs when the potential gets closer to a few kT of the standard potential. After this, the analyte starts to oxidize at the working electrode surface, causing the current to grow exponentially (b). The pace at which the oxidant diffuses to the electrode and the percentage that is transformed into the reduced form determine the current.

This is governed by Nernst equation. The amount of oxidized species present on the surface gradually decreases as the potential sweep progresses, creating a concentration gradient. The distinctive peak seen in the voltammogram is caused by this changing gradient at the electrode interface.

At point c, the current attains its maximum value referred to as the anodic peak current (i_{pa}) at the corresponding anodic peak potential (E_{pa}).

The rate at which the analyte diffuses from bulk solution to electrode surface, which is a relatively slow process on the electrochemical timescale, determines the current after point c. As the potential sweep proceeds toward more positive values, the current declines to point d. A diffusion-controlled steady state is eventually reached, after which further current cannot be produced by further increases in potential.

The analyte is still being oxidized when the scan is reversed to negative potentials (reductive scan). Re-reduction can occur for the oxidized analyte present on the electrode surface (e) until the applied voltage approaches that value.

The reduction process is similar to the oxidation process. The cathodic peak (i_{pc}) at the cathodic peak potential (E_{pc}) (f) and the opposite scan direction are the sole differences [29],[30].

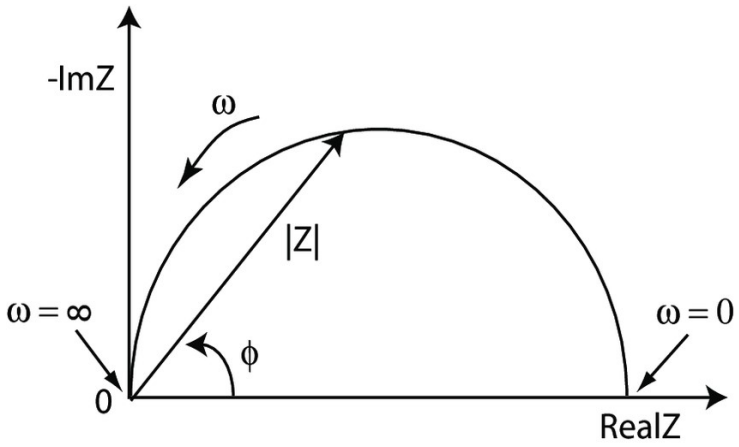

Fig 2.8 Electrochemical impedance spectroscopy

2.5.3 Electrochemical impedance spectroscopy (EIS)

Electrochemical impedance spectroscopy (EIS) is a specialized characterization technique that measures the impedance of an electrochemical system across a range of AC frequencies. In glucose sensing applications, EIS is utilized to regulate interfacial variation at the electrode surface that occur due to glucose oxidation. When glucose interacts with the electrode, it induces changes in charge transfer resistance (R_{ct}), double-layer capacitance (C_{dl}), and warburg impedance, which can be modeled using equivalent circuits (e.g., randles circuit).

These impedance variations are directly correlated with glucose concentration, enabling highly sensitive and selective detection.

Electrochemical impedance spectroscopy (EIS) is typically conducted under open-circuit voltage (OCV) conditions using a small alternating current (AC) signal, usually between 5 and 10 millivolts. The frequency of this signal is varied across a wide range, commonly from 0.1 Hz to 100 kHz. The resulting impedance (Z) reflects the AC resistance of the system and is expressed as a complex number: $Z = Z' + jZ''$, where Z' is the real part and Z'' is the imaginary part. The real component (Z') indicates the resistive aspects of the system, while the imaginary component (Z'') corresponds to its capacitive and inductive characteristics. The nyquist plot is the most commonly used method for analyzing EIS data. It displays the imaginary component of impedance (Z'') plotted against the real component (Z') [32].

2.5.5 Current time (i-t) amperometry

In current time (i-t) amperometry, a fixed voltage is applied to the working electrode, and the current that results is measured over time. After stepping the potential from a non-reactive value to one at which the target analyte is oxidized or reduced, the faradaic current initially spikes and then decays under diffusion control [33].

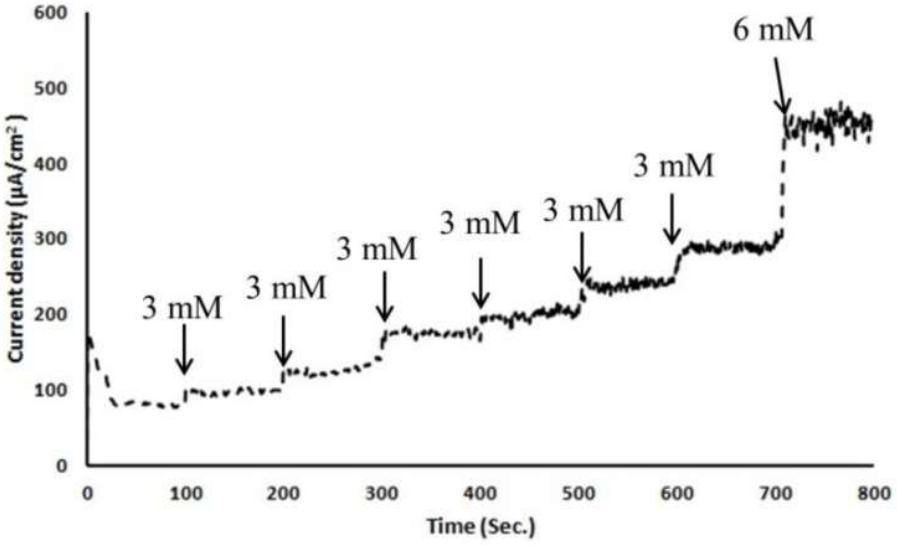

Fig 2.9 Current time (i-t) amperometric curve [34]

CHAPTER - III
CADMIUM HYDROXIDE THIN FILM BY CHEMICAL BATH DEPOSITION METHOD FOR GLUCOSE SENSING APPLICATION

3.1 Introduction

Recently, non-enzymatic sensors have gained significant research interest due to their superior stability, high sensitivity, fast response time, and ease of fabrication compared to conventional enzymatic sensors [35]. These sensors have demonstrated remarkable performance owing to their ability to operate without the need for fragile biological elements, such as enzymes, which are prone to denaturation and instability under harsh conditions [36], [37]. As a result, non-enzymatic sensors are considered highly promising for real-time monitoring, clinical diagnostics, environmental analysis, and wearable electronics. Based on their sensing mechanisms, non-enzymatic glucose sensors typically rely on either direct electrocatalytic oxidation or surface adsorption processes, as discussed in chapter I. Unlike enzymatic sensors, non-enzymatic electrodes often exhibit prominent redox peaks in cyclic voltammetry (CV) measurements, indicating efficient electron transfer and enhanced catalytic activity [38]. These advantages enable non-enzymatic sensors to offer improved durability, broader operating ranges, and higher reproducibility, making them ideal candidates for the next generation of glucose sensing technologies.

3.2 Experimental details

3.2.1 Materials

Cadmium chloride monohydrate ($CdCl_2.H_2O$) (loba, purity 99%), ammonia solution (merck, 28-30%), glucose ($C_6H_{12}O_6$) (SRL, 98%), fructose ($C_6H_{12}O_6$) (SRL, 98%), sucrose($C_{12}H_{22}O_{11}$) (merck, 28-30%) and stainless steel (SS) (304 grade, 46 gauge).

3.2.2 Coating of cadmium hydroxide thin film

$Cd(OH)_2$ thin films are deposited on stainless steel substrates from a prepared cadmium hydroxide solution via chemical bath deposition (CBD).

3.2.2 (a) Substrate selection and cleaning process

To fabricate the glucose sensor electrode, the substrate plays a vital role. When selecting a substrate, it must be conductive, lightweight, flexible, cost-effective, easily available and it should not interfere with the sensing process. Commonly used substrate materials in glucose sensor applications include ITO, nickel foam, graphite sheet, stainless steel, and other conductive metals. In this study, we have chosen stainless steel (SS) due to its affordability and good electrical conductivity. However, stainless steel surfaces are often contaminated, which can hinder the effective immobilization of sensing materials and interfere with the electrochemical response. Therefore, thorough cleaning of the substrate is essential to eliminate surface impurities, promote proper adhesion of the active sensing layer, and ensure a uniform and stable film, ultimately enhancing the sensor's sensitivity and reliability.

Substrate cleaning process

1. **Surface polishing:** Stainless steel substrates (3.5 cm × 5 cm) were polished using sandpaper to smoothen the surface and remove any attached impurities.
2. **Cleaning with detergent:** The substrates were cleaned with labolene detergent and rinsed thoroughly with double-distilled water (DDW) to remove any organic contaminants.
3. **Ultrasonic treatment:** The substrates underwent ultrasonication in DDW for 30 minutes, with the cleaning beaker pre-washed using acid and labolene.
4. **Final rinse and drying:** After ultrasonication, the substrates were rinsed with DDW and dried completely to ensure a clean, residue-free surface.

3.2.2 (b) Material preparation

For the preparation of the cadmium hydroxide $Cd(OH)_2$) solution, 2.05 grams (0.1 M) of monohydrated cadmium chloride ($CdCl_2.H_2O$) was dissolved in 90 ml of DDW. To adjust the pH and facilitate the desired chemical reaction, a few drops of 28% ammonium hydroxide (NH_4OH) was added to cadmium chloride solution,

ensuring the proper conditions for subsequent processing. Resulting a precursor which was used for deposition of $Cd(OH)_2$ on stainless steel substrate [39].

Following reaction happens:

$$CdCl_2.H_2O + NH_4OH \rightarrow Cd(OH)_2 + 2NH_4Cl + H_2O \quad \ldots. (3.1)$$

3.2.3 Thin film on stainless steel by chemical bath deposition method.

Cadmium hydroxide $Cd(OH)_2$ thin film was deposited on a stainless steel (SS) substrate using a simple chemical bath deposition (CBD) method at room temperature. In brief, 0.1 M cadmium chloride ($CdCl_2$) solution was prepared and ammonia (NH_4OH, 28%) was added while stirring. Ammonia acted as a complexing agent, dissolving the initial white precipitate and raising the pH to ~12. After 10 minutes of stirring, the SS substrate was placed in solution and left at room temperature for 16 hours, allowing $Cd(OH)_2$ nanowires to grow on it. The film was then rinsed with double-distilled water, air-dried, and used for future analysis and glucose sensing applications.

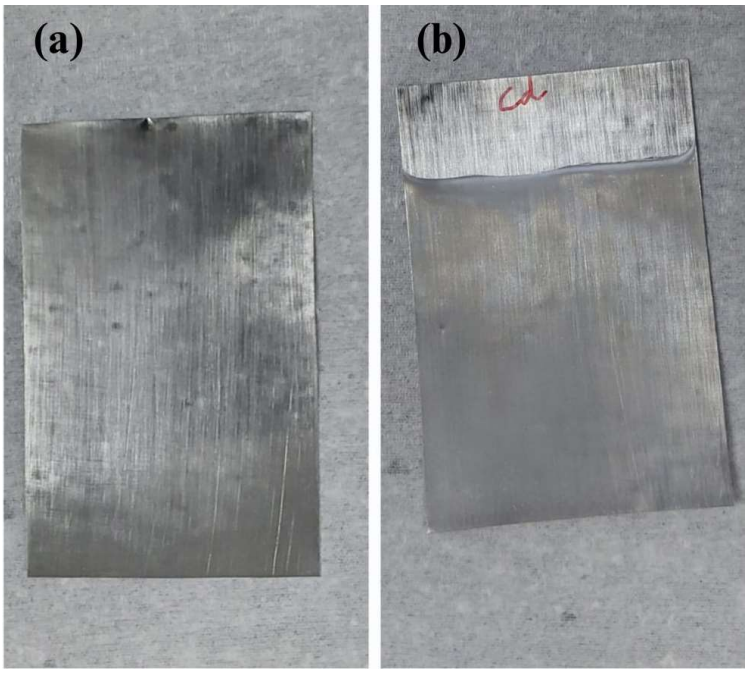

Fig 3.1 (a) Stainless steel substrate (SS) (b) SS/ $Cd(OH)_2$

3.3 Characterizations

The crystal structure of the prepared samples was analyzed using a bruker D2-phaser X-ray diffractometer with Cu-Kα radiation (λ = 1.5406 Å). Fourier transform infrared (FTIR) spectra were recorded using a thermo fisher scientific iS50 instrument within the wavenumber range of 4000 to 400 cm^{-1}. Electrochemical studies, including cyclic voltammetry (CV), current time (i-t) amperometry, and electrochemical impedance spectroscopy (EIS), were performed. The electrochemical measurements were carried out using a gamry interface 1010 E system, employing Ag/AgCl as the reference electrode, $Cd(OH)_2$ as the working electrode (WE), and platinum wire as the counter electrode (CE).

3.4 Results and discussion

3.4.1 XRD structural analysis

The structural characterization of cadmium hydroxide $Cd(OH)_2$ was studied using X-ray diffraction (XRD) analysis, employing stainless steel (SS) as the reference substrate. The recorded XRD patterns of $Cd(OH)_2$, synthesized by the chemical bath deposition method onto SS, are depicted in Figure 3.2.

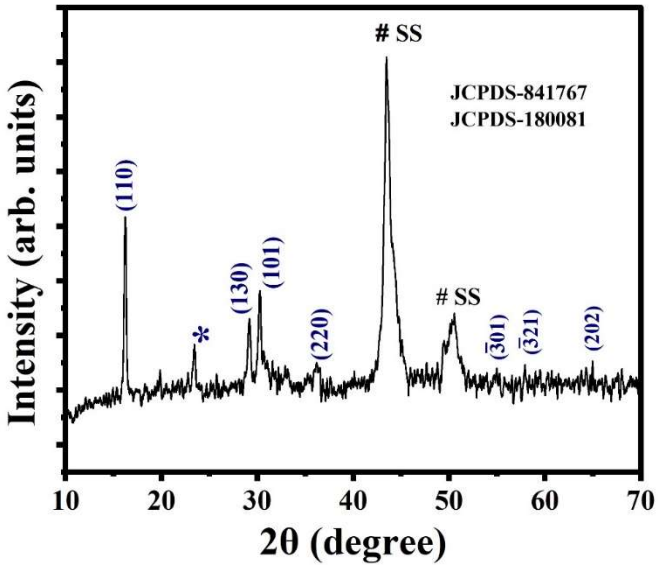

Fig. 3.2 XRD spectra of $Cd(OH)_2$

The diffraction data for both the ammonium chloride and $Cd(OH)_2$ films, intended for glucose sensing applications, were matched the standard joint committee on powder diffraction standards (JCPDS) cards 84-1767. The XRD profile of $Cd(OH)_2$ revealed seven prominent peaks at 2θ values of 16.22°, 29.18°, 30.28°, 36.18°, 54.98°, 57.94°, and 64.98°, which correspond to the monoclinic phase,

associated with the (hkl) planes (110), (130), (101), (220), ($\bar{3}$02), ($\bar{3}$21), and (202) respectively. Furthermore, two characteristic peaks originating from the SS were observed at 43.48° and 50.56°. A distinct peak at 24.56° was also identified, attributed to the presence of residual ammonium cadmium chloride with JCPDS no 18-0081.

Table 3.1 X-ray diffraction peaks position and plane

Sr.No	Angle (2θ) (°)	(hkl) Plane
1	16.22	(110)
2	29.18	(130)
3	30.28	(101)
4	36.18	(220)
5	54.98	($\bar{3}$02)
6	57.94	($\bar{3}$21)
7	64.98	(202)

3.4.2 Fourier transform infrared spectroscopy

Fourier transform infrared (FTIR) spectroscopy is renowned for its exceptional sensitivity, especially in identifying small amounts of inorganic and organic molecules. The FTIR spectrum is presented in figure 3.3.

The FTIR spectrum reveals several characteristic absorption bands. A prominent band observed at 3480 cm^{-1} is attributed to bending vibrations of water molecules as well as the stretching vibrations of O–H bonds, indicating the presence of hydroxyl groups. Another significant absorption peak appears at 1400 cm^{-1}, which is associated with the stretching vibrations of N–H bonds. Furthermore, a strong and broad band located in the lower wavenumber region, specifically around 650

cm^{-1}, is linked to the bending vibrations of Cd–O–H groups, suggesting the formation of cadmium-hydroxide interactions.

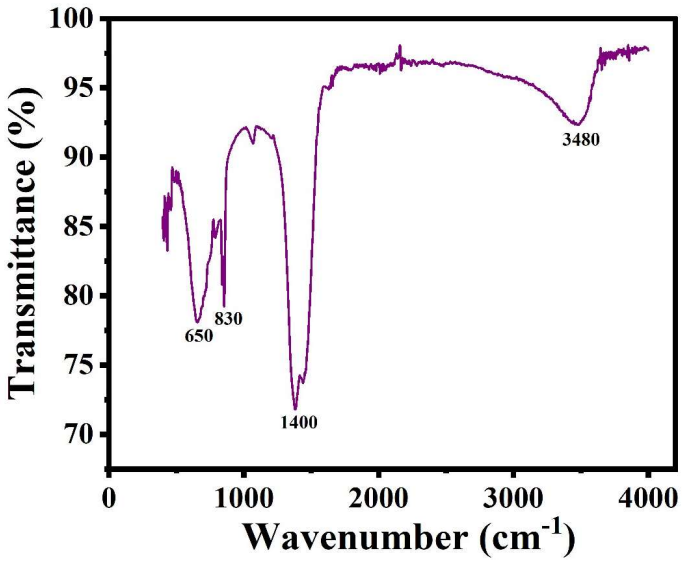

Fig. 3.3 FTIR spectra of $Cd(OH)_2$

Detailed FTIR study confirm that synthesized cadmium hydroxide nanowires not only exhibit these characteristic vibrations but also contain N–H bonds that are intercalated within the hydroxide matrix, providing deeper insights into their structural composition. [40]

3.4.3 Surface morphological studies

The surface morphology of the $Cd(OH)_2$ films was investigated via FESEM. Figure 3.4 presents the SEM image captured from the surface of the sample. The image shows a dense and interconnected network of thin, wire-like structures characteristic of nanowire formations observed on stainless steel (SS) substrate.

The nanowires exhibit a random, entangled arrangement, forming a porous and surface area for glucose sensing application.

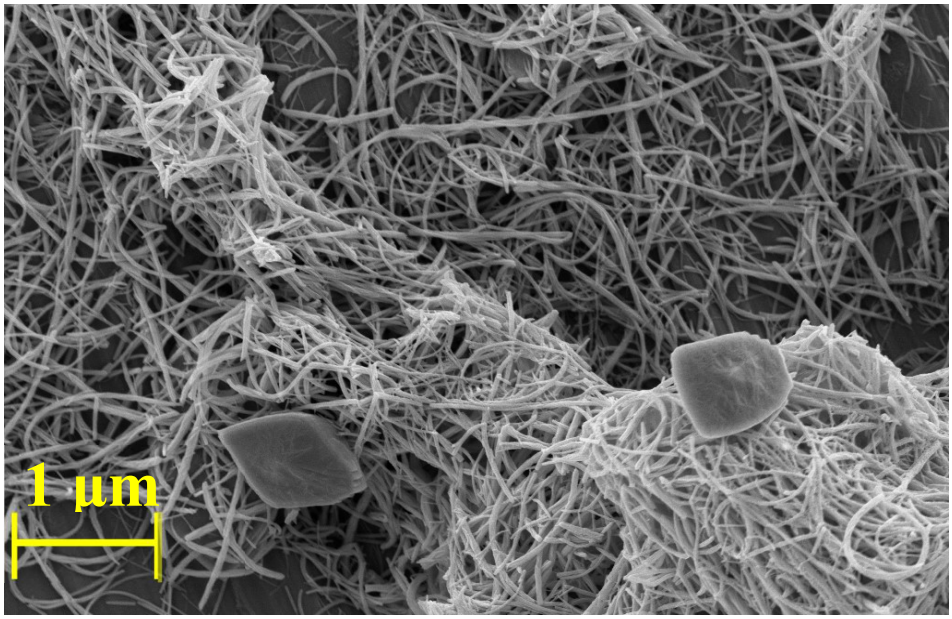

Fig. 3.4 FESEM image of $Cd(OH)_2$ thin film

3.4.3.1 Energy dispersive X-ray spectroscopy (EDX)

Energy dispersive X-ray spectroscopy (EDX) was employed to analyze the elemental composition of the synthesized cadmium hydroxide nanowires, and the resulting spectrum is presented in Figure 3.5. The EDX analysis reveals distinct peaks attributed to cadmium (Cd) and oxygen (O), confirming the presence of these elements within the sample. Quantitative evaluation indicates that the sample consists of 64.57 weight % cadmium and 35.43 weight % oxygen. In terms of atomic percentage, oxygen constitutes 79.40 %, whereas cadmium accounts for 20.60 %.

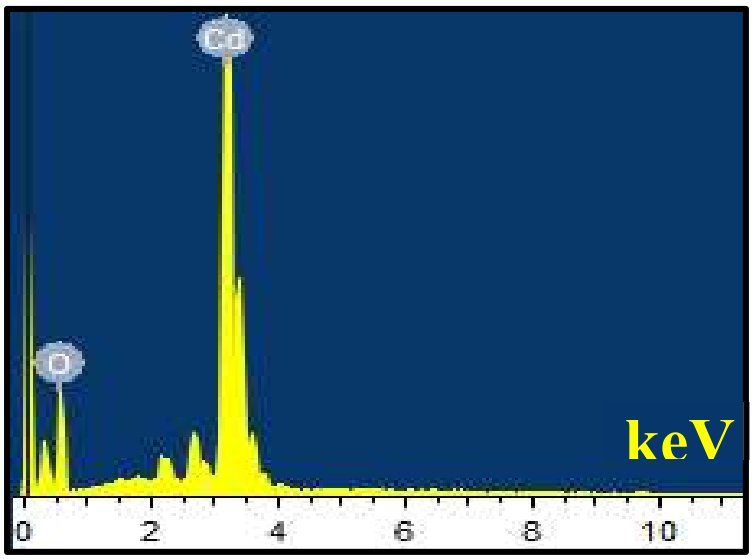

Fig. 3.5 EDX spectra of $Cd(OH)_2$.

Table 3.2 Elemental composition of $Cd(OH)_2$

Element	Weight %	Atomic %
O K	35.43	79.40
Cd L	64.57	20.60
Totals	100.00	

The absence of any detectable impurity peaks suggests a high level of purity in the synthesized material. These data correspond closely to the expected stoichiometry of cadmium hydroxide and further validate the successful formation of the nanowire structure.

3.5 Electrochemical analysis

3.5.1 Sensitivity study

3.5.1.1 Cyclic voltammetry

In order to examine the electrochemical performance of the SS/$Cd(OH)_2$ electrode, cyclic voltammetry (CV) measurements were conducted. Figure 3.6 (a) presents the CV curves of $Cd(OH)_2$ in various electrolytes. The CV profiles were recorded for different electrolytes, each at a fixed concentration of 1 M and a scan rate of 100 mV/s, to determine the electrolyte that yields the highest current density. For the optimisation of the glucose sensor electrode, SS/$Cd(OH)_2$, aqueous solutions of KOH, NaCl, LiCl, Na_2SO_4, and KCl were employed. Among these, 1 M NaCl exhibited the highest current density, as evident from Figure 3.6 (a). This results from fast ion migration, the increased porosity of the interfacial layer caused by chloride adsorption, and the absence of competing side reactions.

Subsequently, further optimization was performed by varying the concentration of NaCl, as illustrated in Figure 3.6 (b). Anodic current remains low at low NaCl levels since the ionic strength is too weak for adequate conductivity. Conductivity and redox kinetics peak with increasing Na+/Cl+, however excess ions restrict mass transport and block active sites, resulting in a modest decrease in current.

Cyclic voltammetry studies of the SS/$Cd(OH)_2$ electrode at different scan rates 100, 75, 50, 25, 10, and 1 mV/s were carried out in a 1 M NaCl electrolyte, within

a constant potential window of 0.8 V (ranging from -0.1 V to -0.8 V), as shown in Figure 3.6(c). The correlation between higher scan rates and increased current density points to a rapid electron transfer process at the electrode interface. Furthermore, a linear relationship between anodic peak current and scan rate, depicted in Figure 3.6 (d), was observed. The obtained slope value of 0.3 shows that diffusion process primarily governs the electrochemical reaction mechanism [17].

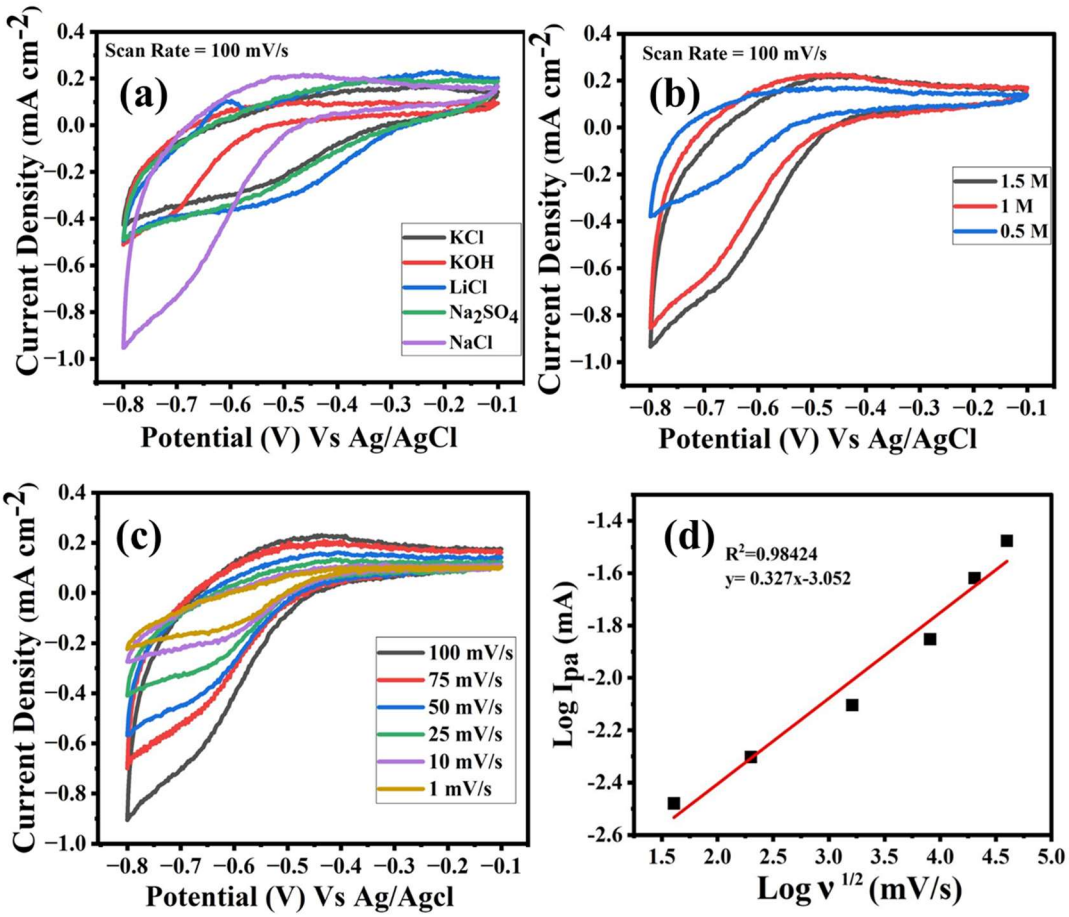

Fig 3.6 (a) Electrolyte variation at the concentration of 1 M, (b) Concentration variation of NaCl electrolyte, (c) CV curves at various scan rates in 1 M NaCl,(d) Peak current vs square root of scan rate in 1 M NaCl

As the glucose concentration increases, distinct oxidation and reduction peaks become more prominent and anodic peak current increases, demonstrating the excellent electrode's activity in catalyzing glucose oxidation, depicted in fig 3.7 (a) & (b).

The gradual rise in anodic peak current with higher glucose levels indicates efficient electron transfer kinetics and high surface sensitivity of the electrode. Additionally, the observed enhancement and shifting of peaks reflect a strong interaction between glucose molecules and the active catalytic sites of the SS/$Cd(OH)_2$ electrode.

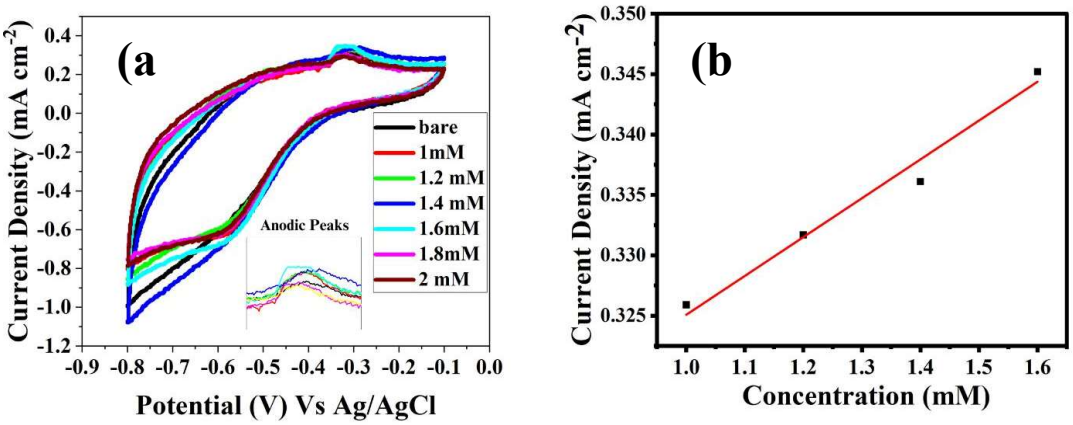

Figure 3.7 (a) CV response of SS/$Cd(OH)_2$ electrode at different concentration of glucose in NaCl Solution & (b) a linear relationship between anodic peak current density and glucose concentration

3.5.1.2 Current time (i-t) amperometry

The chronoamperometric trace in the figure 3.8 illustrates the typical current time (i-t) response of a glucose sensor under successive additions of glucose at a fixed

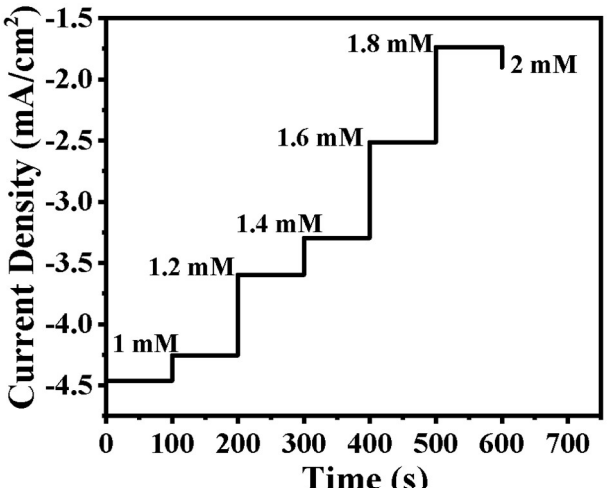

Fig. 3.8 Current time (i-t) amperometric curve of $Cd(OH)_2$ with successive addition of glucose in 1 M NaCl

0.35 V. At time zero, the potential of the electrode is shifted to its operating value and the current decays from an initial spike down to a baseline of approximately –4.5 mA/cm² in pure $Cd(OH)_2$. When 1.0 mM glucose was injected, the oxidation current jumps and stabilizes around –4.3 mA/cm²; each subsequent 0.2 mM increment (to 1.2, 1.4, 1.6, 1.8, and finally 2.0 mM) produces a discrete upward step in current density (toward less negative values), with steady-state levels of roughly –4.0, –3.7, –3.2, –2.5, and –1.8 mA/cm², respectively.

As glucose concentration goes up, the corresponding current rise indicates the electrode's linear sensitivity to glucose.

3.5.1.3 Electrochemical impedance spectroscopy

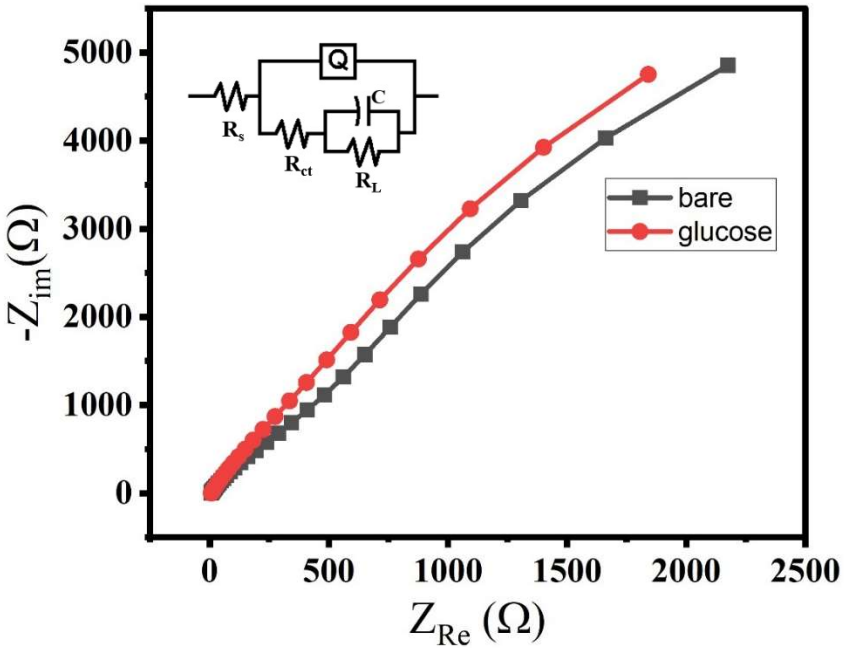

Fig 3.9 Nyquist plot of bare electrode and addition of 1 mM glucose

To study the electrical resistance and charge transfer resistance electrochemical impedance spectroscopy were conducted within the frequency range of 0.1 Hz to 1 MHz. Here the nyquist plot with analogus circuit fitted for SS/$Cd(OH)_2$ in 1M NaCl shown in fig 3.9. In the circuit C, R_s, R_{ct}, Q and R_L stand for double layer capacitance ,solution resistance, charge transfer resistance constant phase element & load resistance respectively.

It shows that with the addition of 1 mM glucose, the solution resistance R_S and charge transfer resistance R_{ct} found to decrease to the values 4.707 (Ω cm^{-2}) and

845.5 (Ω cm^{-2}) respectively as the charge transfer process of the carriers increases due to the oxidation of glucose.

Table 3.3 Impedance parameters

Resistace (Ω cm^{-2})	Bare	SS/$Cd(OH)_2$
R_S	5.559	4.707
R_{ct}	849.2	845.5
R_L	1.709E4	772.7

3.5.2 Selectivity

3.5.2.1 Cyclic voltammetry

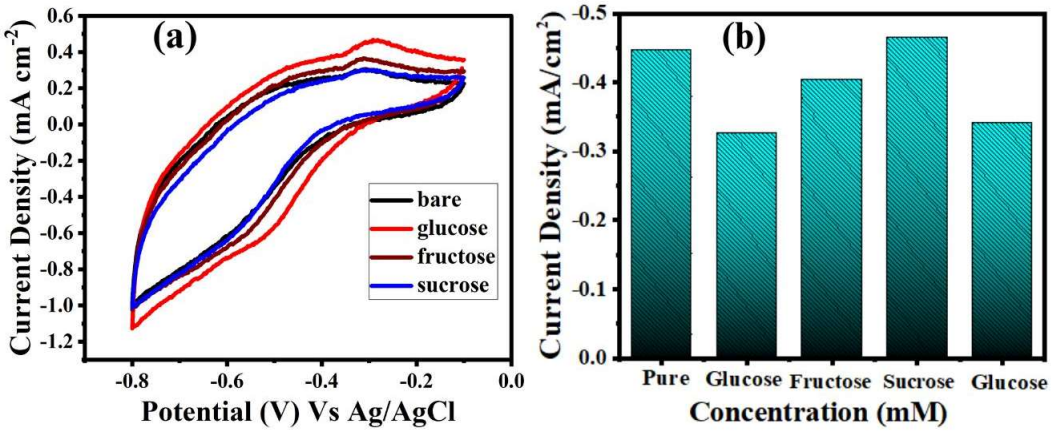

Figure 3.10 (a) CV response of SS/$Cd(OH)_2$ thin film towards glucose selectivity w.r.t fructose, sucrose (b) Variation of current density with concentration for different selective elements

To identify the selectivity of the prepared electrode CV has been done in the presence of fructose, sucrose at a concentration of 1 mM in 1 M NaCl electrolyte as shown in fig 3.10(a) and fig3.10 (b). The bare electrode shows a very small oxidation peak & in the presence of glucose, got the highest peak showing good selectivity of the electrode as the aldehyde group in glucose can be oxidized directly on the $Cd(OH)_2$ film. As it is tiny and only contains one sugar, it adheres to the surface and moves more quickly than larger sugars.

3.5.2.2 Current time (i-t) amperometry

Further to see the further selectivity of electrode, amperometry was conducted in presence of other selective elements like fructose, sucrose at a concentration of 1 mM in 1 M NaCl electrolyte

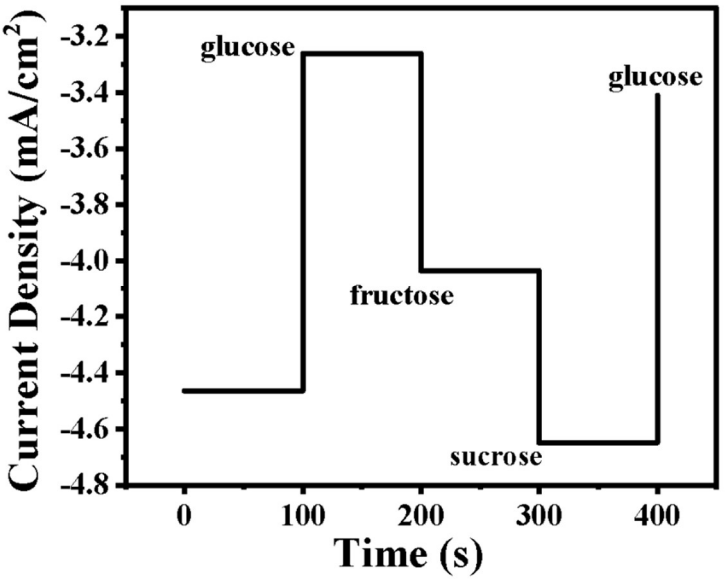

Fig. 3.11 Current time (i-t) amperometric curve of $Cd(OH)_2$ in presence fructose sucrose at a concentration of 1 mM in 1 M NaCl electrolyte

Fig 3.11 displays that glucose additions produce a large jump in current density, indicating a strong oxidation. Fructose and sucrose cause small changes, showing that these sugars do not oxidize significantly at our electrode under these conditions. On again addition of glucose, the second glucose pulse reproduces the initial current increase, confirming the electrode's reversible and linear response to glucose.

CHAPTER IV
SUMMARY AND CONCLUSIONS

4.1 Introduction

Thin film techniques provide an effective and reliable route for the synthesis of nanomaterials. Cadmium hydroxide ($Cd(OH)_2$) is deposited on a suitable substrate using the chemical bath deposition (CBD) method. As discussed in chapter 2, thin films can be prepared using both physical and chemical methods. However, many of these methods such as sputtering, evaporation, and plasma-enhanced chemical vapor deposition require expensive setups and complex operations. Therefore, the CBD method is favored due to its low cost, ease of processing, and capability to produce uniform nanostructured films under mild conditions. The deposited $Cd(OH)_2$ films are further optimized and studied for glucose sensing applications, where their high surface area and electrochemical activity enhance sensitivity and performance. The completed project is divided into four parts, including the following.

1. Chapter 1: The first chapter contains a brief overview about glucose sensing & different types of it. In particular, we have focused our work on non enzymatic sensors as they provide selectivity and rapid results. Further, previous works on glucose sensing were summarized in the form of a tabular column.

2. Chapter 2: This chapter reviews the theoretical foundations of thin-film deposition and the various characterization techniques. It begins with a classification of thin films, outlines the principles of chemical bath deposition, and summarizes the key preparative parameters and their benefits. It then describes the structural, morphological, and electrochemical analysis methods employed—namely X-ray diffraction (XRD), scanning electron microscopy (SEM), fourier-transform infrared spectroscopy (FTIR), cyclic voltammetry (CV), current–time (i–t) amperometry, and electrochemical impedance spectroscopy (EIS).

3. Chapter 3: This chapter focuses on the preparation and evaluation of the $Cd(OH)_2$ electrode. The electrode was fabricated via chemical bath deposition, and its crystal phase was examined by X-ray diffraction (XRD). Additionally, the chapter presents the electrochemical performance studies conducted on the $Cd(OH)_2$ electrode.

4.2 Results and discussion

4.2.1 Characterization analysis

4.2.1.1 X-ray diffraction

- Peaks at 16.22°, 29.18°, 30.28°, 36.18°, 54.98°, 57.94°, 64.98° align with known $Cd(OH)_2$ planes indicates purity of the sample with monoclinic crystal structure
- Sharp, distinct peaks indicate high crystallinity with minimal defects.
- Asterisk marked peak is due to ammonim cadmium hydroxide at minute level

4.2.1.2 Fourier transform infrared spectroscopy

- The wide band at 3480 cm^{-1} corresponds to O–H stretching and water bending vibrations.
- The band near 1400 cm^{-1} arises from N–H stretching vibrations.
- The peak at 650 cm^{-1} is attributed to Cd–O–H bending modes.
- Absence of other peaks (e.g., carbonate or nitrate) suggests minimal contamination.

4.2.1.3 Scanning electron microscope (SEM)

- A dense, uniform layer of nanowires of $Cd(OH)_2$ covers the stainless-steel substrate
- There is a agglomeration of wires
- EDX spectra has confirmed the existence of cadmium and oxygen in the sample

4.2.1.3 Electrochemical study

Table 4.1 Maximum anodic current of $Cd(OH)_2$ in different electrolytes at 100 mV/s.

Sr.No	Electrolyte	Maximum anodic current (mA cm^{-2})
1	KCl	0.101
2	KOH	0.089
3	LiCl	0.100
4	Na_2SO_4	0.124
5	NaCl	0.208

- The highest anodic current occurs in NaCl, indicating optimal ion transport and surface reactions in this medium.
- Na_2SO_4, LiCl & KCl showing that they still support good anodic activity but less effectively than NaCl.
- KOH gives the smallest current implying that strongly basic conditions may hinder the anodic oxidation kinetics of $Cd(OH)_2$.

Table 4.2 Maximum anodic current of $Cd(OH)_2$ in different concentration of NaCl.

Sr. No	Concentration (M)	Maximum anodic current (mA cm^{-2})
1	0.5	0.162
2	1	0.229
3	1.5	0.220

- At low concentration, limited ionic strength leads to poorer conductivity and slower charge transfer, so the anodic current is lower.
- Sufficient Na^+/Cl^- ions boost solution conductivity and facilitate redox reactions at the electrode, giving the highest current.
- Excess ions may hinder mass transport and blocking active sites causing a slight drop in anodic current

Table 4.3 Maximum anodic current of $Cd(OH)_2$ with different scan rates

Sr.No	Scan rate (mV/s)	Maximum anodic current (mA cm^{-2})
1	1	0.075
2	10	0.085
3	25	0.112
4	50	0.154
5	75	0.182
6	100	0.221

- Peak anodic current grows with the scan rate showing a clear positive dependence on scan speed.
- The increase roughly follows a $\sqrt{v}$ trend, indicating that the redox reaction is restricted by ion diffusion to the electrode surface.
- Faster scans shorten the diffusion layer thickness, boosting the instantaneous flux of ions and thus the anodic current.

Table 4.4 Maximum anodic current of $Cd(OH)_2$ in different concentration of glucose

Sr. No	Concentration (mM)	Maximum anodic current (mA cm^{-2})
1	bare	0.266
2	1	0.202
3	1.2	0.213
4	1.4	0.226
5	1.6	0.308
6	1.8	0.242
7	2.0	0.316

- Upon increasing the glucose concentration, the electrocatalytic activity of the $Cd(OH)_2$ electrode increases indicates the increase enhanced mass-transport flux.

Table 4.5 Maximum anodic current of $Cd(OH)_2$ in various selective elements

Sr. No	Selective elements	Maximum anodic current (mA cm^{-2})
1	Fructose	0.364
2	Sucrose	0.306
3	Glucose	0.4662

- Highest current in glucose shown by glucose because it's a simple sugar that oxidizes easily on $Cd(OH)_2$.
- Medium current in fructose; similar size to glucose but a different structure makes it slightly harder to oxidize.
- Lowest current in sucrose; it's a larger disaccharide that must break apart before oxidizing, slowing the reaction.

Table 4.6 Impedance parameters

Resistace (Ω cm^{-2})	**Bare**	**SS/$Cd(OH)_2$**
R_s	**5.559**	**4.707**
R_{ct}	**849.2**	**845.5**
R_L	**1.709E4**	**772.7**

- The addition of glucose causes all the impedance parameters to drop as electrocatalytic activity of SS/Cd(OH)2 rises with the oxidation of glucose, hence unrestricted transfer of charge carriers.

4.3 Conclusions

The $Cd(OH)_2$ thin film in nanowire form was synthesized via a simple, cost-effective chemical bath deposition (CBD) method at room temperature. Electrochemical cyclic voltammetry (CV) measurements in 1 M NaCl solution revealed oxidation peaks and a high electrocatalytic current density, indicating efficient electron transfer at the film interface. Chronoamperometric studies demonstrated excellent selectivity toward glucose, with negligible response to common interfering species in NaCl background. The optimized $Cd(OH)_2$ is suitable for rapid and selective glucose sensing in saline environments.

References

[1] E. Renard, “Monitoring glycemic control: the importance of self-monitoring of blood glucose,” Am J Med, vol. 118, no. 9, pp. 12–19, Sep. 2005, doi: 10.1016/j.amjmed.2005.07.052.

[2] L. Tang, S. J. Chang, C. J. Chen, and J. T. Liu, “Non-invasive blood glucose monitoring technology: A review,” Dec. 01, 2020, MDPI AG. doi: 10.3390/s20236925.

[3] “E. L. Lundgrin, C. A. Kelly, N. Bellini, C. Lewis, E. Rafi, and B. Hatipoglu, “Diabetes Technology Trends: A review of the latest innovations,” The Journal of Clinical Endocrinology & Metabolism, vol. 110, no. Supplement_2, pp. S165–S174, Jan. 2025, doi: 10.1210/clinem/dgaf034

[4] H. Lee, Y. J. Hong, S. Baik, T. Hyeon, and D. H. Kim, “Enzyme-Based Glucose Sensor: From Invasive to Wearable Device,” Adv Healthc Mater, vol. 7, no. 8, Apr. 2018, doi: 10.1002/adhm.201701150.

[5] V. B. Juska and M. E. Pemble, “A critical review of electrochemical glucose sensing: Evolution of biosensor platforms based on advanced nanosystems,” Nov. 01, 2020, MDPI AG. doi: 10.3390/s20216013.

[6] M. H. Hassan, C. Vyas, B. Grieve, and P. Bartolo, “Recent advances in enzymatic and non-enzymatic electrochemical glucose sensing,” Jul. 02, 2021, MDPI AG. doi: 10.3390/s21144672.

[7] S. B. Jadhav et al., “Effect of Mn doping on electrochemically synthesized Mn-La_2O_3 thin films non-enzymatic glucose sensor,” Journal of Materials Science: Materials in Electronics, vol. 34, no. 1, Jan. 2023, doi: 10.1007/s10854-022-09399-9.

[8] G. A. Naikoo et al., “Non-enzymatic glucose sensors composed of trimetallic CuO/Ag/NiO based composite materials,” Sci Rep, vol. 13, no. 1, Dec. 2023, doi: 10.1038/s41598-023-32719-w.

[9] S. Guo et al., “A facile and sensitive electrochemical sensor for non-enzymatic glucose detection based on three-dimensional flexible polyurethane sponge decorated with nickel hydroxide,” Anal Chim Acta, vol. 1109, pp. 130–139, May 2020, doi: 10.1016/j.aca.2020.02.037.

[10] N. I. Chandrasekaran and M. Manickam, “A sensitive and selective non-enzymatic glucose sensor with hollow Ni-Al-Mn layered triple hydroxide nanocomposites modified Ni

foam," Sens Actuators B Chem, vol. 288, pp. 188–194, Jun. 2019, doi: 10.1016/j.snb.2019.02.102.

[11] V. Osuna, E. P. Aparicio Martínez, R. B. Dominguez, and A. Vega Rios, "A Review on the Advances in Nanomaterials for Electrochemical Non-Enzymatic Glucose Sensors Working in Physiological Conditions," Aug. 01, 2024, Multidisciplinary Digital Publishing Institute (MDPI). doi: 10.3390/chemosensors12080159.

[12] S. Karmakar, S. K. Kundu, S. K. Bandyopadhyay, M. Gangopadhyay, and G. S. Taki, "Importance of transition metal modified graphene-based non-enzymatic blood glucose sensors," in 2020 4th International Conference on Electronics, Materials Engineering & Nano-Technology (IEMENTech), IEEE, Oct. 2020, pp. 1–4. doi: 10.1109/IEMENTech51367.2020.9270049.

[13] H. Li, L. Zhang, Y. Mao, C. Wen, and P. Zhao, "A Simple Electrochemical Route to Access Amorphous Co-Ni Hydroxide for Non-enzymatic Glucose Sensing," Nanoscale Res Lett, vol. 14, 2019, doi: 10.1186/s11671-019-2966-2.

[14] B. Fall et al., "Highly efficient non-enzymatic electrochemical glucose sensor based on carbon nanotubes functionalized by molybdenum disulfide and decorated with nickel nanoparticles (GCE/CNT/MoS_2/NiNPs)," Sensors and Actuators Reports, vol. 5, p. 100136, Jun. 2023, doi: 10.1016/j.snr.2022.100136.

[15] Z. Haghparas, Z. Kordrostami, M. Sorouri, M. Rajabzadeh, and R. Khalifeh, "Highly sensitive non-enzymatic electrochemical glucose sensor based on dumbbell-shaped double-shelled hollow nanoporous CuO/ZnO microstructures," Sci Rep, vol. 11, no. 1, Dec. 2021, doi: 10.1038/s41598-020-79460-2.

[16] G. A. Naikoo et al., "Non-enzymatic glucose sensors composed of trimetallic CuO/Ag/NiO based composite materials," Sci Rep, vol. 13, no. 1, Dec. 2023, doi: 10.1038/s41598-023-32719-w.

[17] S. B. Jadhav et al., "Effect of Mn doping on electrochemically synthesized Mn-La_2O_3 thin films non-enzymatic glucose sensor," Journal of Materials Science: Materials in Electronics, vol. 34, no. 1, Jan. 2023, doi: 10.1007/s10854-022-09399-9.

[18] Y. Bai, W. Yang, Y. Sun, and C. Sun, "Enzyme-free glucose sensor based on a three-dimensional gold film electrode," Sens Actuators B Chem, vol. 134, no. 2, pp. 471–476, Sep. 2008, doi: 10.1016/j.snb.2008.05.028.

[19] H. Li, L. Zhang, Y. Mao, C. Wen, and P. Zhao, "A Simple Electrochemical Route to Access Amorphous Co-Ni Hydroxide for Non-enzymatic Glucose Sensing," Nanoscale Res Lett, vol. 14, 2019, doi: 10.1186/s11671-019-2966-2.

[20] Z. Haghparas, Z. Kordrostami, M. Sorouri, M. Rajabzadeh, and R. Khalifeh, "Highly sensitive non-enzymatic electrochemical glucose sensor based on dumbbell-shaped double-shelled hollow nanoporous CuO/ZnO microstructures," Sci Rep, vol. 11, no. 1, Dec. 2021, doi: 10.1038/s41598-020-79460-2.

[21] G. A. Naikoo et al., "Non-enzymatic glucose sensors composed of trimetallic CuO/Ag/NiO based composite materials," Sci Rep, vol. 13, no. 1, Dec. 2023, doi: 10.1038/s41598-023-32719-w.

[22] Y. Bai, W. Yang, Y. Sun, and C. Sun, "Enzyme-free glucose sensor based on a three-dimensional gold film electrode," Sens Actuators B Chem, vol. 134, no. 2, pp. 471–476, Sep. 2008, doi: 10.1016/j.snb.2008.05.028.

[23] Libretexts, "X-ray diffraction (XRD) basics and application," Chemistry LibreTexts, https://chem.libretexts.org/Courses/Franklin_and_Marshall_College/Introduction_to_Materials_Characterization__CHM_412_Collaborative_Text/Diffraction_Techniques/X-ray_diffraction_(XRD)_basics_and_application (accessed May 14, 2025).

[24] Technical note: Introduction to FTIR spectroscopy, FT-IR Spectroscopy, https://www.newport.com/n/introduction-to-ftir-spectroscopy (accessed May 14, 2025).

[25] M. R. Mahadeshwara, "Fourier Transform Infrared Spectroscopy - about tribology." https://www.tribonet.org/wiki/fourier-transform-infrared-spectroscopy/

[26] V. Profile, SCANNING ELECTRON MICROSCOPE (SEM) - Working principle and applications, Feb. 08, 2023. https://microsaranraj.blogspot.com/2023/02/scanning-electron-microscope-sem.html

[27] C. Song, J. Guo, Y. Wang, H. Xiang, and Y. Yang, "Electrochemical Glucose Sensors: Classification, catalyst innovation, and sampling mode evolution," Biotechnology Journal, vol. 19, no. 10, Oct. 2024, doi: 10.1002/biot.202400349.

[28] Kalara Develigoda Gamage, The EIS analysis of a) three-electrode system, b) two-electrode systems...|download scientific diagram, https://www.researchgate.net/figure/The-EIS-analysis-of-a-three-electrode-system-b-two-electrode-systems-with-full-cell_fig5_327816295 (accessed May 14, 2025).

[29] "Potentiostat Quickstart guide," Ossila. [Online]. Available: https://www.ossila.com/pages/cyclic-voltammetry

[30] “Cyclic Voltammetry: Basic principle - Chemistry Notes,” Chemistry Notes, Jul. 12, 2022. https://chemistnotes.com/physical/cyclic-voltammetry-basic-principle/

[31]BioLogic, “What is Electrochemical Impedance Spectroscopy (EIS)? Electrochemistry Basics Series - BioLogic Learning Center,” BioLogic, Jan. 14, 2025. https://www.biologic.net/topics/what-is-eis/

[32]Susan Amrose, Addy, and Addy, Electrochemical arsenic remediation for rural Bangladesh, https://www.researchgate.net/figure/A-simple-Nyquist-plot-showing-complex-impedance-vector-Zo-Note-that-the-Y-axis-is_fig8_241588665 (accessed May 14, 2025).

[33] A. Amine, H. Mohammadi, and Elsevier Inc., “Amperometry,” in Encyclopedia of Analytical Science, P. Worsfold, A. Townshend, and C. Poole, Eds. Elsevier, 2020, pp. 70–79. [Online]. Available: https://doi.org/10.1016/B978-0-12-409547-2.14204-0

[34] Y. Yoon, G. Lee, K. Yoo, and J.-B. Lee, “Fabrication of a Microneedle/CNT Hierarchical Micro/Nano surface electrochemical sensor and its In-Vitro glucose Sensing characterization,” Sensors, vol. 13, no. 12, pp. 16672–16681, Dec. 2013, doi: 10.3390/s131216672.

[36] Author links open overlay panelKathryn E. Toghill and An overview of glucose sensors is presented, “Electrochemical non-enzymatic glucose sensors: A perspective and an evaluation,” International Journal of Electrochemical Science, https://www.sciencedirect.com/science/article/pii/S1452398123153594 (accessed May 14, 2025).

[37] C. Chen et al., “Recent advances in electrochemical glucose biosensors: a review,” RSC Advances, vol. 3, no. 14, p. 4473, Dec. 2012, doi: 10.1039/c2ra22351a.

[38] D.-W. Hwang, S. Lee, M. Seo, and T. D. Chung, “Recent advances in electrochemical non-enzymatic glucose sensors – A review,” Analytica Chimica Acta, vol. 1033, pp. 1–34, May 2018, doi: 10.1016/j.aca.2018.05.051

[39] A. A. Mancharkar et al., “Cadmium hydroxide nanowires for high performance supercapacitor by chemical bath deposition,” ES Energy & Environments, Jan. 2023, doi: 10.30919/esee1048.

[40] S. L. Patil, S. S. Raut, and B. R. Sankapal, “$Cu(OH)_2$@$Cd(OH)_2$ core-shell nanostructure: Synthesis to supercapacitor application,” Thin Solid Films, vol. 692, p. 137584, Oct. 2019, doi: 10.1016/j.tsf.2019.137584.